Authors' response:

We carefully considered the referee#1's suggestions drawing our attention to the agricultural emissions which finally turned out to be determining the post-2006 methane increase, totally camouflaging tropical wetlands and NH fossil sources.

Paper update:

Text:

L 193-195:

The contributions by enhanced release from tropical wetlands, North American shale gas drilling (FracFocus, 2016), and agriculture are discussed in Sect. 4.2 and displayed in Fig. S2c.

New **Figure** for supplement (Fig. 2) replacing 2. 1,b):

New **Table**:

As required by the co-editor we summarized the statistics in Table 3:

The referee suggested the following references for consideration:

Nisbet et al. (2016):
The increasing production of fossil fuels to some extend may explain the CH4 trend; however, by means of 13C/ 12C (CH_4) data and a box model concluded that fossil fuel related emissions are a minor contributor to the renewed methane increase, compared to agricultural emissions dominated by ruminants and rice.

Schaefer at al. (2016):
[…] tropical wetland emissions, […] match the post-2006 perturbation not as well as emissions from rice cultivation and (C3-fed) ruminants.
However, this isotopic evidence against tropical wetlands is not strong . . .

Mikaloff-Fletcher and Schaefer (2019):
"whereas fossil CH4 emissions from North America remained flat despite a nearly 50% increase in natural gas production (11)."

We followed the suggestion and expanded our study with the two agricultural scenarios: enhanced emissions from ruminants and those from rice paddies, both based on the same geographical source distributions as assumed for the years before 2007.

Including the two additional hypotheses we optimized the emission scenarios sha (US shale gas fracking), tro (tropical wetlands), ani (animals / ruminants), and ric (rice paddies) and all possible combinations which include a contribution from sha, wrt smallest RMS-deviation and highest R^2 at 16 NOAA-stations.

The results are in full agreement with the conclusions of the publications quoted by the referee. We did not change any of the simulations described in the previous version but just expanded the number of hypothetical scenarios by rice cultivation and ruminant animal emissions as required.

Text modifications:

Abstract	L 31-39
Introduction	L 65- 97

2.3.1 Methane emissions L 194

4 Simulation results L 262- 269

4.2 Simulating the recent methane trend L396 – 479

5. Conclusions L 537-554

New References L696 and L744

Model simulations of atmospheric methane 1997-2016 and their evaluation using NOAA and AGAGE surface- and IAGOS-CARIBIC aircraft observations

Peter H. Zimmermann[1], Carl A. M. Brenninkmeijer[1], Andrea Pozzer[1], Patrick Jöckel[3], Franziska Winterstein[3], Andreas Zahn[2], Sander Houweling[4], and Jos Lelieveld[1]

[1]Max Planck Institute for Chemistry, Department of Atmospheric Chemistry, Mainz, Germany
[2]Karlsruhe Institute of Technology (KIT), Institute for Meteorology and Climate Research, Karlsruhe, Germany
[3] Deutsches Zentrum für Luft- und Raumfahrt (DLR), Institut für Physik der Atmosphaere, Oberpfaffenhofen, Germany
[4] Netherlands Institute for Space Research, Utrecht, the Netherlands

Correspondence to: Peter H. Zimmermann (p.zimmermann@mpic.de)

Abstract.

The global budget, variability and trend of atmospheric methane (CH_4) have been simulated with the EMAC atmospheric chemistry – general circulation model in specified dynamics mode for the period 1997 through 2016. Observations from seventeen AGAGE and NOAA surface stations and intercontinental CARIBIC flights indicate a transient period of declining methane increase during 1997 through 1999, followed by seven years of stagnation and a sudden resumed increase after 2006.

Starting the simulation with a global methane distribution that matches the station measurements in January 1997, and using inter-annually constant CH_4 sources from eleven categories together with photochemical and soil sinks, the model reproduces the CH_4 observations during the transient and constant period from 1997 through 2006 in magnitude as well as seasonal and synoptic variability.

The atmospheric CH_4 dry air mole fractions in our model setup without chemical feedback on the reactants are linearly dependent on the source strengths, allowing the source segregated simulation of eleven biogenic and fossil emission categories (tagging), with the aim to analyze global observations and derive the source specific CH_4 steady state lifetimes (τ). Moreover, tagging enables a-posteriori rescaling of individual emissions with proportional effects on respective source segregated methane abundances. A sophisticated optimization procedure ("Solver") was applied to the model results minimizing the Root Mean Square deviation (RMS) from the observations. Under given constraints the 2000 – 2006 observed all-station mean dry air mole fraction of 1,780 nmol/mol could be reproduced within an RMS = 0.40 %, associated with a coefficient of determination R^2 = 0.81. With regard to source optimization this implies a reduction in fossil fuel (predominantly coal and gas) related emissions and an increase in biogenic sources such as tropical wetlands and rice paddies. The observed interhemispheric difference between the most northerly and southerly stations was reproduced within 0.76 %.

The CH_4 rise started nearly linearly from 2007 through 2013, explained by an additional emission of 20.47 Tg/y CH_4. We explored the contributions of four potential causes, representing biogenic emissions from tropical wetlands (TRO), from agriculture including ruminant animals (ANI) and rice cultivation (RIC), and from anthropogenic (e.g. shale gas fracturing) fossil emissions from North America (SHA), added to the posteriori no-trend period emission distribution. For each source, independently, between 20.36 and 20.64 Tg/y were obtained with the Solver to fit the observed trend with smallest RMS. A statistically most likely combination completely excludes the fossil source SHA in favor of 20.02 Tg/y CH_4-RIC and a small addition of 0.43 Tg/y CH_4-TRO.

After 2013 the trend steepened and further assumptions will be needed, not discussed in this study.

Nearly 800 CH_4 samples gathered during 95 intercontinental CARIBIC flights in the upper troposphere and lower stratosphere (UTLS) in the period 1997-2006 were simulated within RMS = 1.1 % deviation from the mean CH_4 mixing ratio, mostly over the Northern Hemisphere. While measurements were quite disperse in time, the relatively continuous India flight record between 1997 and 2001 was reproduced within an RMS = 0.98 % and $R^2 = 0.65$. Similarly, more than 4,000 samples collected during 232 CARIBIC flights after 2007 were simulated with an RMS = 1.30 %. The coefficient of determination $R^2 = 0.80$ implies that the model reproduces 80 % of the seasonal and synoptic variability of CH_4 in the UTLS. The slope of the linear regression analysis with 0.58 however indicates underestimation of the calculated CH_4 variability because the vertical resolution of the model grid is not sufficient to resolve the fine structure of the tropopause region.

1 Introduction

The greenhouse gas methane (CH_4) is emitted into the atmosphere by various natural and anthropogenic sources, and is removed by photochemical reactions and to a small extent through oxidation by methanotrophic bacteria in soils (Dlugokencky et al., 2011). The tropospheric mean lifetime of CH_4 due to oxidation by OH has been estimated to be 8-9 years (Lelieveld et al., 2016) and its concentration has been growing by about 1 %/y since the beginning of the Anthropocene in the 19th century (Crutzen, 2002, Ciais et al. 2013).

The resulting factor of 2.5 increase in the global abundance of atmospheric methane (CH_4) since 1750 contributes 0.5 Wm^{-2} to total direct radiative forcing by long-lived greenhouse gases (2.8 Wm^{-2} in 2009), while its role in atmospheric chemistry adds another approximately 0.2 Wm^{-2} of indirect forcing (Dlugokencky et al., 2011). Etminan et al. (2016) presented new calculations including the impact of the shortwave forcing and found that the 1750–2011 radiative forcing is about 25% higher (increasing from 0.5 Wm^{-2} to 0.6 Wm^{-2}) compared to the value in the Intergovernmental Panel on Climate Change (IPCC) 2013 assessment. After the strong upward CH_4 trend since the 1960s, by the end of the 1990s the increase had slowed down until sources and sinks quasi balanced for about 8 years, while in 2007 the CH_4 increase resumed unexpectedly (Bergamaschi et al., 2013). Fig. 1 demonstrates the development of the CH_4-mixing ratio at the NOAA observation site South Pole (SPO, 90° S) over the years 1997 through 2016, the period considered in this modeling study, and reveals a no-trend period from 2000 through 2006.

The resuming upward trend after 2007 (Dlugokencky et al., 2009; Rigby et al., 2008, IPCC 2014) is not fully understood (Nisbet et al., 2014, Mikaloff-Fletcher and Schaefer, 2019), and causes of the trend changes have been subject of a number of studies, some with contradictory results, highlighting the complexity of the processes that control atmospheric methane in the Anthropocene.

Data analysis (Nisbet et al., 2016, Worden et al., 2017) and inverse modelling studies (Bergamaschi et al., 2013) indicate that global emissions since 2007 were about 15 to 25 Tg CH_4/y higher than in previous years, possibly caused by increasing tropical wetland emissions and anthropogenic pollution in mid-latitudes of the northern hemisphere.

Hausmann et al. (2016), using methane and ethane column measurements, concluded that the increase in CH_4 since 2007 has been between 18 to 73 % (depending on assumed ethane/methane source ratios) due to thermogenic methane. Further, Helmig et al. (2016) suggested a large contribution of US oil and natural gas production to the increased emissions. A potentially growing source that was identified is hydraulic shale gas fracturing, for instance in Utah, where 6 to 12 % of the natural gas produced may locally leak to the atmosphere (Karion et al., 2013, Helmig et al. 2016).

At first glance the increasing production of fossil fuels may explain the CH_4 trend but it was concluded (Schwietzke et al., 2016) that overall fossil sources have decreased during the last decades owing to industrial efficiency improvements. Based on $^{13}C/^{12}$ C isotope ratio analyses for 2007-2011 Schaefer at al. (2016) concluded that fossil fuel related emissions are a minor contributor to the renewed methane increase, compared to tropical wetlands and agriculture.

According to Nisbet et al. (2016) "since 2007 $\delta^{13}C$-CH_4 (a measure of the $^{13}C/^{12}$ C isotope ratio in methane) has shifted to significantly more negative values suggesting that the methane rise was dominated by increases in biogenic methane emissions, particularly in the tropics, for example, from expansion of tropical wetlands in years with strongly positive rainfall anomalies or emissions from increased agricultural sources such as ruminants and rice paddies". With regard to biogenic emission sources, e.g. Saunois et al. (2016) conclude that "methane emissions from increasing agricultural activities seem to be a major, possibly dominant, cause of the atmospheric growth trends of the past decade" and "Recent bottom-up inventories estimate an increase in annual agricultural emissions of 3–5 Tg between 2006 and 2012, mostly from Africa and Asia, whereas wetland emissions were estimated to be mostly unchanged between 2006 and 2012". In this context Schaefer et al. (2016) state that "after 2006, the activation of biogenic emissions caused the renewed CH_4 rise", thus raising concern about the contribution from rice production versus wetland emissions. The latter are higher in the southern hemisphere, whereas remote sensing shows that CH_4 mainly increased in the northern tropics and subtropics (Houweling et al., 2014). Furthermore, tropical wetlands match the post-2006 $\delta^{13}C$-CH_4 perturbation not as well as rice cultivation and C3-fed ruminants (Schaefer et al., 2016).

Here we investigate how well, based on source estimates, CH_4 mixing ratios and their changes over the past two decades can be simulated numerically, by accounting for atmospheric dynamical and chemical processes with the ECHAM/MESSy Atmospheric Chemistry (EMAC), which describes the transport, dispersion, and chemistry of atmospheric trace constituents, and allows the online sampling of calculated mixing ratios in four dimensions, mimicking the sampling by observational systems (Jöckel et al., 2010). To evaluate the simulation results we use CH_4 measurements at surface stations, i.e. data from NOAA (Dlugokencky et al., 2018) and AGAGE (Prinn et al., 2000) and CH_4 data collected by the CARIBIC (Civil Aircraft for the Regular observation of the atmosphere Based on an Instrumented Container) passenger aircraft (Brenninkmeijer et al., 2007).

Both measurement data sets (i.e. the surface-station and the aircraft based) allow a global approach, with each having its characteristic "footprint". The station data are based on regular measurements at fixed coordinates in both hemispheres. The CARIBIC data are based on monthly flight series (nominally 4 sequential long-distance flights) covering large parts of the globe from a Eurocentric perspective.

A summary of all abbreviations is provided in the "Acronyms" table at the end.

2 Model Setup

2.1 The EMAC numerical model

The EMAC model is a chemistry and climate simulation system that includes sub-models describing tropospheric and middle atmosphere processes and their interaction with oceans, land and human influences. The Modular Earth Submodel System (MESSy, www.messy-interface.org) results from an open, multi-institutional project providing a strategy for developing comprehensive Earth System Models (ESMs) with flexible levels of complexity. MESSy describes atmospheric chemistry and meteorological processes in a modular framework, following strict coding standards. The sub-models in EMAC have been coupled to the 5th generation European Centre HAMburg general

circulation model (ECHAM5, Röckner et al., 2006), of which the coding has been optimized for this purpose (Jöckel et al., 2006, 2010).

The extended EMAC model version 2.50 at T106L90MA resolution was used to simulate the global methane budget. A triangular truncation at wave number 106 for the spectral core of ECHAM5 corresponds to a ~1.1°×1.1° horizontal quadratic Gaussian grid spacing near the equator, and 90 levels on a hybrid-pressure grid in the vertical direction span from the Earth's surface to 0.01 hPa pressure altitude (~80km, the middle of uppermost layer). The vertical resolution near the tropopause is about 500 m. Numerical stability criteria require an integration time step of 1-2 min. With regard to model dynamics, we applied a weak "nudging" towards realistic meteorology over the period of interest, more specifically by Newtonian relaxation of four prognostic model variables temperature, divergence, vorticity and the logarithm of surface pressure towards ERA interim data (Dee et al., 2011) of the European Centre for Medium-range Weather Forecasting (ECMWF).

Apart from the prescribed sea surface temperature (SST), the sea-ice concentration (SCI), and the nudged surface pressure, the nudging method is applied in the free troposphere only, tapering off towards the surface and the tropopause, so that stratospheric dynamics are calculated freely, and possible inconsistencies between the boundary layer representations of the ECMWF and ECHAM models are avoided. Further, in the free troposphere, the nudging is weak enough to not disturb the self-consistent model physics, while this approach allows a direct comparison of the model output with measurement data (without constraining the model physics), and therefore offers an efficient model evaluation.

The EMAC sub-model collection includes "CH4" (Frank, 2018) which is tailored for stratospheric and tropospheric methane chemistry and solves the ordinary differential equations describing the oxidation of methane by OH, O^1D, Cl and photolysis. The feedback to the hydrological cycle by modification of the specific humidity is optional in CH4 and was switched off in this particular setup for the same reason as applying tropospheric nudging as mentioned above.

The sub-models "SCOUT" and "S4D" enable online sampling of model parameters such as tracer mixing ratio at selected observation sites as well as along aircraft measuring flight routes (http://www.messy-interface.org/ "MESSy Submodels" and Jöckel et al., 2010).

2.2 Model setup for Methane budget investigation

As long as the tracers under consideration are not subject to chemical feedback reactions among each other, they can be processed like separate tracers. In this manner, atmospheric methane can be tagged e.g. by the source category which they derive from and can be simulated individually, while their sum exactly fits the simultaneous total CH_4 calculations. In our particular case, no feedback is affecting the prescribed OH distribution neither in the gross nor in the tagged mode. (cf. Sec. 2.3.3). The water that is produced by methane oxidation in the used setup was not added to the hydrological cycle because this is only relevant in the stratosphere.

The sub-models "SCOUT" and "S4D" enable online sampling of model parameters such as tracer mixing ratio at selected observation sites as well as along aircraft measuring flight routes (http://www.messy-interface.org/ "MESSy Submodels" and Jöckel et al., 2010).

Using a priori emission estimates, an initial CH_4 distribution was derived in the course of several spin-up simulations repeated until a steady state global CH_4 mass has settled over the years 1997 through 2006.

The module "Solver" is a spreadsheet optimizer that is bundled with Microsoft Excel (Fylstra et al. 1998) and uses the "Generalized Reduced Gradient method" (GRG) (Lasdon et al. 1978). A "goal function" defined by the user can be optimized under given constraints upon specific parameters.

In this modeling study the Solver is applied to post-process eleven tagged source segregated a priori tracer distributions (CH_4^i, i = 1, … , 11). The Solver calculates scale factors c^i with the aim to minimize the Root Mean Square deviation (RMS) of $\sum (c^i\, CH_4^i)$ from the observations CH_4^O evaluated at selected ground stations. Constraints have to be imposed under plausibility considerations to avoid unrealistic solutions.

2.3 Methane sources and sinks

2.3.1 Methane emissions

The combined input from eleven inter-annually constant natural and anthropogenic methane source types amounts to 580 $TgCH_4$/y, applied to the simulation period 1997 – 2016 (Table 1, col. 3).

Anthropogenic and natural methane sources are based on The Global Atmospheric Methane Synthesis (GAMeS), a GAIM/IGBP (http://gaim.unh.edu/) initiative to develop a process-based understanding of the global atmospheric methane budget for use in predicting future atmospheric methane burdens. Emission data for this initiative have been used for the model setup described here. Natural wetland emissions are based on Walter et al. (2000), fossil sources based on EDGARV2.0 and remaining sources as compiled by Fung et al. (1991). Processes with similar isotopic characteristics are aggregated into one group. Oil related sources, for example, comprise mining and processing of crude fuel and all emission classes related to the use of fossil fuel such as residential heating, on/offshore traffic, industry, etc., and also include an estimate of volcanoes (Houweling et al., 1999). Given that methane emissions from boreal/arctic wetlands are quite uncertain, it is reasonable to assume that this source category accounts for permafrost decomposition emissions as well.

The "burning"-part of the GAMeS dataset is replaced by the GFEDv4s statistics (Randerson et al., 2018) in addition to biofuel combustion emissions from the EDGARV2.0 database (Olivier, 2001). The biogenic emissions from bogs, rice fields, swamps and biomass burning are subject to seasonal variability. About 60 % of the total emissions of 580 Tg/y are caused by human activities; the remainder is from natural sources. At northern middle and high latitudes, methane sources predominantly comprise animals (ruminants), bogs, gas and coal production, transmission and use, landfills, and boreal biomass fires. Tropical wetlands (partly in the subtropics) are the world's largest (natural) source of methane together with animals. Minor tropical anthropogenic input is from biofuel combustion. The individual source strengths are partly subject to seasonal variability, and except for inter-annual differences in the ~20 Tg/y biomass burning, are assumed to be inter-annually constant in a reference simulation for the full period 1997 through 2014. More illustrative plots are provided in the supplement, such as Fig. S1a,b, which depicts the total emission distribution in g (CH_4) /m^2 /month for Jan. (a) and Jul. (b), in logarithmic scale for better representation, to illustrate seasonal CH_4 changes.

A rearrangement among the natural wetland and the anthropogenic landfill-, coal-, gas-, and oil contributions by ~20 $Tg(CH_4)/y$ (i.e. 3.6 % of the total) in favor of biogenic emissions such as low latitude wetlands and rice paddies has been applied retrospectively under the condition of least RMS deviation between station and model CH_4 mixing ratios.

The horizontal resolution of all methane fluxes is 1°×1°. Because biomass burning emissions are associated with thermal uplift, they are vertically distributed up to 3000 m altitude and higher according to a profile suggested in EDGAR3.2ft (Aardenne et al., 2005). The GFEDv4 biomass burning statistics include agricultural waste burning events. Biomass burning emissions are inter-annually variable and the 1997 emission was 2.4 times as high as the 1998-2015 average (Fig. S1c).

Additional emission sources are necessary to close the budget during the methane rising period after 2006. The contributions by enhanced release from tropical wetlands, ruminant animals, rice paddies, and North American shale gas drilling (FracFocus, 2016) are discussed in Sect. 4.2 and displayed in Fig. S2.

2.3.2 Methane uptake by soils

A small but significant (6.6 % in this study) removal process of methane is its oxidation by methanotrophic bacteria in soils (Dlugokencky et al., 2011). The MESSy sub-model "DDEP" simulates dry deposition of gas phase tracers and aerosols (Kerkweg et al. 2006). For our CH_4 budget modeling the deposition velocity was derived for a fixed atmospheric-methane mixing ratio of 1800 nmol/mol (Spahni R. et al., 2011, Ridgwell et al., 1999) and is scaled correspondingly. The deposition has a pronounced seasonal cycle in phase with the wetland emissions and depends on soil temperature, moisture content and the land cultivation fraction and varies from 2.4 Tg in January to 4.0 Tg in July.

2.3 Methane chemical removal

The chemical removal process of CH_4 is photo-oxidation, predominantly by hydroxyl (OH) radicals. In addition to the reaction with OH in the troposphere and stratosphere, there are minor oxidation reactions with atomic chlorine (Cl) in the marine boundary layer and the stratosphere and with electronically excited oxygen atoms ($O(^1D)$) in the stratosphere (Lelieveld et al., 1998; Dlugokencky et al., 2011). In EMAC the methane photolysis and chemical reaction system is numerically solved by the sub-model "CH4". Global distributions of OH, Cl, and $O(^1D)$ have been pre-calculated from the model evaluation reference simulation S1 (Jöckel et al., 2006), therefore providing internally consistent oxidation fields for the model transport and chemistry of precursors. Monthly averaged fields calculated for the year 2000 have been used in this study.

3 Observations used for model evaluation

The EMAC model simulates the global distribution of methane from given emission source categories, and produces time series of methane distributions as output. Additionally, model samples during the simulation are recorded for the evaluation of the results at prescribed locations and times. Monthly averaged mixing ratios are computed at the location of selected NOAA and AGAGE sites and about 4,600 CARIBIC flight measuring samples (Brenninkmeijer et al., 1999, 2007) gathered during more than 350 flights from 1997 through 2014. The station records predominantly serve as a reference for the model- and recursive emission evaluation and help to gain confidence in the CARIBIC flight data analysis and interpretation.

3.1 NOAA and AGAGE station network

The NOAA Global Greenhouse Gas Reference Network measures the atmospheric distribution and trends of the three main long-term drivers of climate change including methane (CH_4), the subject of this study. The Reference Network is part of NOAA's Earth System Research Laboratory in Boulder, Colorado (https://www.esrl.noaa.gov/gmd/ccgg/).
The data provided (Dlugokencky et al., 2018) are filtered with respect to synoptic scale pollution events. We take advantage of 16 stations approximately equally distributed over the globe (Fig. 2a) and remote from the major emission areas to ensure comparability with the model results which are not filtered. For the same reason, in case of Cape Grim, Australia (41° S, 145°) we refer to the unfiltered AGAGE records (Prinn et al., 1978, 2013). At all stations monthly mean mixing-ratios are compared to respective monthly averaged model samples.

3.2 CARIBIC flight observations

CARIBIC (Civil Aircraft for the Regular Investigation of the Atmosphere Based on an Instrument Container, Brenninkmeijer et al., 2007) is a European passenger aircraft based atmospheric composition monitoring project that has become part of the IAGOS Infrastructure (www.iagos.org). CARIBIC deploys an airfreight container equipped with about 1.5 tons of instruments, connected to a multi-probe air inlet system. The container is installed monthly for 4 sequential measurement flights from and back to Frankfurt or Munich Airport after which air samples, aerosol samples and data are retrieved. The container houses instruments for measuring ozone, carbon monoxide, nitrogen oxides, water vapor and many more trace gases as well as atmospheric aerosols. Air samples are collected at cruise altitudes between about 10 and 12 km and depending on latitude and season and actual synoptic meteorological conditions represent tropospheric or stratospheric air masses.

Overall the ratio between sampled stratospheric and tropospheric air masses is about 0.5. These air samples are analyzed in the laboratories of the CARIBIC partner community. More than 40 gases are measured including hydrocarbons, halocarbons and greenhouse gases including CH_4. Methane mixing ratios were determined at coordinates along flight tracks over regions such as Europe (EUR), North America (NAM), South America – north (SAN), South America – south (SAS), Africa (AFR), India and Indonesia (IND), and Far East (FAE) and color coded in Fig. 2b. These values, interpolated in time and space onto the model grid, are subject of our evaluation.

The calibration is carried out using NOAA Methane WMO scale (Dlugokencky et al., 2005) For further information about CARIBIC based studies involving CH_4, we refer to Schuck et al. 2012, Baker et al. 2012, and Rauthe-Schöch et al. 2016. For the period 1997-2002, we use data from the first phase of CARIBIC (Brenninkmeijer et al. 1999).

4 Simulation results

Starting with a global distribution derived from spin-up simulations (Sect. 2), a time series of the monthly mean global methane distribution up to December 2016 has been calculated together with online samples at the seventeen ground stations and along the CARIBIC flight tracks for comparison. Characteristic features, such as global CH_4 distributions and seasonal cycles as well as the local variability of station and flight records can be successfully reproduced for the first three years 1997 – 1999, during the slowing increase, as well as the subsequent period through 2006 without a trend.

In our specific model setup, the oxidation chemistry, neglecting chemical feedback reactions on the oxidants as well as on H_2O, responds linearly to the emissions, thus allowing the separate tracer simulation of individual sources by tagging. Consequently, the sum of eleven tagged methane tracers exactly reflects the reference total methane distribution, and the CH_4 composition at any grid point in the atmosphere can be attributed to the specific source categories. Furthermore, the tagging retrospectively allows re-scaling the source segregated a-priory global methane distributions with the aim of an optimal station measurement fitting approach – Sect. 4.1.1.

For the trend period since 2007 we introduced additional emissions to account for the recent CH_4 increase (Kirschke et al., 2013, Miller et al., 2013, Nisbet et al., 2016, Turner et al., 2017). On top of the rescaled “base” emissions from the non-trend years we simulated the effect of four tagged potentially rising biogenic sources: tropical wetlands, ruminant animals, rice cultivation, and a new fossil emission source from North America based on shale gas drilling statistics. Also for this period the smallest RMS (measurement vs model) deviation together with the coefficient of determination R^2 is used as a criterion to evaluate the emission scenarios, while the Solver optimization analysis attributes an overwhelming ~ 99% to biogenic agricultural (see Sect. 4.2 for more details).

4.1 The period 1997 through 2006

For initialization, a global methane distribution pattern for January was created as mentioned above (Sect. 2.2) and ensures a balanced annual average global CH_4 mass over the entire period with inter-annually constant sources and sinks up to deviations caused by variations in biomass burning. According to prescribed 4-dimensional coordinate tables, calculated CH_4 mixing ratios are recorded and stored at all sampling positions and times at selected (NOAA (Dlugokencky, 2018) and AGAGE (Prinn et al., 2013) observation sites and along the CARIBIC flight tracks (Brenninkmeijer et al., 1999, 2007) for the years 1997 through 2016 in view of further graphical and statistical evaluation. Additionally, based on the mass conserving sources in the EMAC model simulation, for the entire time period a series of global CH_4-distributions was produced and stored in 2-day frequency.

The linear dependency between source strength and atmospheric abundance in this model setup (see 2.2) ensures that the sum of all tagged tracers – as mentioned above – is equal to the reference tracer comprising the sum of all emissions. Moreover, this numerical property of the model's partial differential equation system allows the redistribution of certain amounts among – e.g. northern and southern – emitters without affecting the global budget.

While the global total CH_4 emissions are relatively well-constrained, estimates of emissions by source category range within a factor of two (Dlugokencky et al. 2011). The global observational networks have shown to be very helpful to derive the emissions at large scales. The CARIBIC observatory provides an additional global constraint of CH_4 abundance and variability in the UTLS, not directly affected by emission sources at the surface, while being sensitive to the vertical exchange of air masses between the lower and upper troposphere.

The use of tagged tracers helps to determine the origin of the methane that is sampled. Tagged initial distributions and tagged soil sinks are calculated as ratios between the respective source fluxes and the total. Corresponding source-segregated CH_4 station and aircraft samples were calculated the same way as for the reference tracer, but in this case for all categories. Chemical reactions and photolysis were the same for all tagged tracers as for total CH_4, i.e. the tagged emissions are exposed to the same oxidant environment. Assuming that the sources are inter-annually constant, apart from the variability in the comparably small (3.4 %) biomass burning source, the partial masses of the tagged tracers remain in steady state over the simulation period at roughly proportional amounts to the emission fluxes. However, the exact weighting factors, in terms of the steady-state atmospheric lifetimes, vary somewhat around the integral lifetime $\tau \cong 8.45$ years because of different exposures to the major chemical destruction areas. The individual steady state lifetimes are quantified in Sect. 4.1.1 and listed in Tab. 1, col. 5).

The integrated tagged CH_4 masses exactly match the mass of the reference tracer with all sources, which confirms the linearity of the system with chemical feedbacks suppressed through the fixed oxidant distributions. Seasonal global mass variations in individual contributions from constant sources are caused by OH-chemistry and dynamics, e.g. by the migrating ITCZ.

4.1.1 NOAA/AGAGE stations

Based on the a priori emission assumptions (Table 1, col. 3) the 2000 through 2006 average CH_4 mixing-ratio over all AGAGE/NOAA stations of 1,780 nmol/mol is simulated within a Root Mean Square deviation (RMS) of 0.40 %. With the applied initial distribution and emissions, the model reproduces both the 1997-1999 trend and the period without

trend from 2000-2006. This suggests that the global CH_4 concentration in the period 2000-2006 represents the steady state after previously increasing emissions, probably until the early 1990s.

Consistent with the observations, the simulated CH_4 mixing ratios are largest at BRW (71°N) and decrease with latitude, reaching minimum values south of 40 °S at CRZ (46°S), HBA (76°S), and SPO (90°S). The abundance at AGAGE CGO (41°S) is slightly enhanced and scattered, being exposed to pollution events from the Australian continent, but also well reproduced by the model. The 2000-2006 (no-trend period) average observed mean mixing ratios for these stations range from 1,865 to 1,727 nmol/mol and, using a-priori emissions, are simulated within an average percentage RMS = 0.67 %. Northern Hemispheric values however are overestimated, e.g. at BRW by 18.2 nmol/mol (0.98 %) much more than the 5.7 nmol/mol (0.33 %) at SPO (North Pole) and cause an excessive interhemispheric difference (Fig. 3, black crosses vs open blue circles) indicating mismatches in the emission assumptions. Although this imparity could also be caused by erroneous interhemispheric transport, previous analyses (Aghedo et al.2010, Krol et al. 2017) show that the underlying ECHAM5 model reproduce realistically the Inter-hemispheric transport time.

Taking advantage of the Solver (Sect. 2.2) we defined the goal as the minimum RMS deviation between the station measurements and respective model simulations composed of the tagged components multiplied with scaling factors, i.e. the parameters. Likely tolerance intervals (constrains) are available in form of uncertainty specifications along with the a-priori emission assumptions (e.g. Bergamaschi et al., 2013). The largest interval (12%) is allowed for the category gas production.

The a-priori simulation results (Fig. 3, black crosses), as mentioned above, are too high in the Northern Hemisphere compared to the observations (blue circles) suggesting overestimated emission assumptions there. The Solver consequently calculates a 20.6 Tg CH_4 /y reduction of fossil fuel emissions (predominantly coal and gas) in favor of an 18.8 Tg/y increment in the other sources (predominantly tropical wetlands, rice paddies, and biomass burning) to fit the observations. The resulting station mixing-ratios are marked by red dots in Fig. 3. The optimization effect on the emission categories is summarized in Table1, col. 4 and graphically displayed in Fig. S4 (supplement). Hence, the net reduction of just 1.84 Tg/y (0.32 % of the total) underlines the general consistency of the a-priori assumptions, while the necessity of the redistribution among the uncertain emissions by source category (Dlugokencky et al. 2011). The RMS deviation from the all-station average mole fraction improves to 7.17 (0.40 % of the all-station 2000-2005 mean). The all station coefficient of determination $R^2 = 0.80$ confirms the good agreement with observed variability (see scatter plots in Fig. 4 for individual stations ALT, RPB, and SPO, which perform even better). The calculated 2000-2006 average interhemispheric methane difference between extreme NH and SH stations of 131 nmol/mol improves by a factor of 12 and matches the observations up to 0.76 %. Fig. 5 shows the final simulation results based on the revised emissions together with the measurement at five representative observation sites. The initial distribution, which is the result of a long term simulation, does not precisely reflect the special Jan. 1997 situation, but obviously overestimated starting values at northern hemispheric stations level out in the course of the first year. The Solver cannot improve this because it acts on the whole 4d tracer distribution time series and not on individual years.

The tagged tracers indicate that the atmospheric mixing-ratios over the years 1997 through 2006 are proportional to the respective emission amounts, but influenced by the distance from the source due to the oxidation by OH. Footprints at stations are the result of source and sink interaction (Fig. S5). A shorter distance leads to a reduced atmospheric abundance relative to the source strength and vice versa. This is quantified in terms of "steady state lifetime", defined as the ratio between the global atmospheric trace mass (i.e. atmospheric burden) and the annual emission amount, which is , by definition of steady state, equal the total annual sink. Over the period of relative stagnation 2000 – 2006 (Fig. 1)

the shortest lifetimes ($\tau \cong 7.3$ years) were found for fossil methane being emitted predominantly by industrialized countries, from landfills and oil production in the Northern Hemisphere and therefore experiencing the highest OH concentrations (Fig. 6). On the other hand, wetland methane (swamps) is exposed to lower OH concentration, producing a steady state lifetime of $\tau = 10.08$ years (Table 1, col. 5 and Fig. S6a). Biomass burning methane never establishes steady state equilibrium because of the very irregular inter-annual intensity of the fire events (Fig. S6b). Considering that its contribution to the total emissions with ~3.5 % is small, the quantification of the total CH_4-lifetime $\tau \cong 8.45$ years appears reasonable.

From 2007 on, when the station records show an upward trend (cf. Fig. 1 representatively for SPO) additional emissions were necessary in order to close the budget if the sink processes are kept unchanged. The simulation for this period is presented in Sect. 4.2.

4.1.2 CARIBIC flights

The spatio-temporal distribution of the CARIBIC CH_4 sampling is quite different from that of the surface stations. Measurements were taken over relatively short time intervals and more than 96 % of the samples are from the NH. In contrast to the monthly average station data, the CARIBIC individual methane observations in the UTLS are based on air sampling over 20 minutes (i.e. ~300 km) for CARIBIC-1 and about two minutes (i.e. ~30 km) for CARIBIC-2 and compared to the stations appear to be much more variable. The sequence of sampling is irregular in time, i.e. the same destinations are reached through different flight routes (Fig. 2b), and take place during different times of the year. Thus the following statistics are not comparable to the station observations.

Between 2000 and 2006, all CARIBIC observations average at 1,786 nmol/mol. Corrected with respect to the a-posteriori emission data based on the station analysis, the simulation average comes as close as 1,788 nmol/mol. The whole period is fairly well reproduced within an RMS deviation of 1.01 % and a coefficient of determination $R^2 = 0.65$ (Table 3, rows C1-4). The scattered sampling positions cannot be accurately reproduced by the grid model EMAC, because of its limited resolution. The observed CH_4 variability features short-duration events like the interception of methane plumes or alternatively relatively clean air episodes and especially stratospheric air, however, the patterns are rather well reproduced (Fig. 7). The model appears to capture the variations well, even those which are subject to intercepting upper tropospheric and lowermost stratosphere at mid and higher latitudes.

The amplitudes of the model time series, however, are smaller due to the relatively coarse vertical grid spacing of the model, which represents the UTLS at a vertical resolution of about 500m – compared to ~45m near surface. In contrast to background station measurements, for the CARIBIC time series local maxima and minima are not only related to season but also to vertical gradient effects, especially due to the strong concentration changes across the tropopause. The scatter plot (Fig. 8, upper left) shows a regression slope of 0.57, i.e. well below 1, which quantifies the evident underestimation of the calculated CH_4 variability in the graphs of Fig. 7, suggesting that the vertical resolution of the model grid is not optimal to resolve the fine structure in the tropopause region. The slope is compensated by a corresponding offset up to 766 nmol/mol, explaining the good congruence between simulations and observations in Fig. 7.

For further analysis, according to the definition in Sect. 3.2 (Fig. 2b), we grouped the data records in Fig. S7 by the six flight sampling regions: EUR, AFR, FAE, IND, SAN, and SAS (no NAM-flights were performed before 2007). The best agreement between model and observations in terms of RMS is achieved over low-latitude regions such as IND with 0.80 % and SAN/SAS ≤ 0.75. Here the effect of stratospheric air is least. At the same time, observations over

continental areas in the mid latitude NH still could be simulated within a RMS range of 1.23 % (EUR) and 1.24 % (FAE). It appears that the variance of the CARIBIC measurements with $R^2 > 0.60$ is fairly well reproduced everywhere and most accurately over EUR with $R^2 = 0.82$ (Fig. 8). AFR is not discussed here because of the sparse number of samples of 4.7 % of all. The statistics are summarized in (Table 2, rows C1-5).

4.2 Simulating the recent methane trend

The measured methane increase, depicted by the blue lines in Fig. 9a for the NOAA background station data SPO (90°S) and in Fig. 9b for the CARIBIC flight records, cannot be reproduced by the model (red lines) based on inter-annually constant emissions. Between 2007 and 2013 the slope appears nearly linear (Fig. 1), and the discrepancy can be removed by assuming an additional constant CH_4 source for this period. After 2013 the trend steepened and a further increment is required to explain the observations (Mikaloff-Fletcher and Schaefer, 2019). The evaluation of additional emission estimates for that period will be subject of further investigations on the basis of longer time series beyond 2016.

Encouraged by our tagging results, an EMAC model sensitivity study was performed with four hypothetical source categories, namely enhanced emissions from tropical wetlands (scenario TRO), agriculture, i.e. ruminant animals (ANI) and rice cultivation (RIC), and an additional source from North American shale gas drilling (SHA), to resolve the increasing post-2006 model vs. observation discrepancy.

Kirschke et al. (2013) found that an increase by 17-22 Tg/y could explain the renewed methane growth, and Turner et al. (2016), based on satellite retrievals and surface observations, derived that a large increase in U.S. methane emissions could account for 30–60% of the increase.

Enhanced precipitation in the boreal summer season (Nisbet et al., 2016; Bergamaschi et al., 2013) is considered as a possible cause of growing tropical wetland emissions. To create a "fracking" map we relied on the publicly available database maintained by the national hydraulic fracturing chemical registry (FracFocus, 2016). ANI and RIC source regions are assumed to be the same as for the pre-2007 years. Fig. S2 depicts the geographical distribution of the global CH_4 mixing ratios near the surface, logarithmically scaled for better visibility, marking the respective hypothetical sources. At the same intensity SHA and RIC emissions are more spatially concentrated compared to TRO and ANI. Large areas of ANI cover the same region over India as RIC which may be an uncertainty factor in the source attribution analysis. The stronger vertical transport intensity of TRO compared to SHA, leading to reduced altitude gradients (Figs. S3), is related to the proximity to the ITCZ.

We used the same upper limit emission of 28 $Tg/CH_4/y$ to be added in order to fit the upward trend between 2007 and 2013. Separate tagged simulations of TRO, ANI, RIC, and SHA were performed with these sources starting in Jan. 2007. Applying the Solver, the specific annual emission amounts were optimized with respect to RMS deviation from the observations. Except for ANI the coefficient of determination R^2 varies consistently, in a sense that lower RMS deviation is associated with higher R^2. The relatively reduced R^2 of ANI may be due to the neglect of a seasonal distribution.

Consistent with recent $\delta^{13}C\text{-}CH_4$ studies (Schaefer at al., 2016, Schwietzke et al., 2016) biogenic emissions and especially those from rice cultivation (RMS = 0.44 %) best explain the trend observed at the sixteen NOAA stations considered here. Any attempt to find an optimal combination of fractional amounts would be strongly dependent on empirical constraints to be imposed on the individual source strengths and would be rather theoretical. Applying the Solver with “open” limits ($1 \geq e_x \leq 0$) imposed on the emission sources e_x where x = ANI, TRO, SHA, RIC, preventing

tagged source amounts from becoming larger than the total increment or becoming negative, results in a pure biogenic, 98 % RIC and 2 % TRO composition. In the following three sensitivity studies are presented:

In order to consider the suggestion by Turner et al. (2016) with respect to enhanced U.S. methane emissions – see above - we applied a conservative lower limit of 9.0 Tg/y (30 %) to SHA in our statistical evaluation. This is at the expense of RIC (-14.8 Tg/y) and favors TRO (+ 5.9 Tg/y). The RMS (-1.4 %) as well as R^2 (+0.5 %) deteriorate.

The longitudinal dependency of northern hemispheric anthropogenic fossil CH_4 emissions was investigated based on two options: one with the North American source redistributed to East Asia (FAE: 25° N – 50° N, 100° E - 150° E) and another to Europe (EUR: 45°N – 60°N, 0° - 26°E). While no significant trend impact could be assigned to EUR, statistically a hypothetical FAE contribution cannot be excluded. No evidence in favor of SHA or FAE can be detected at one of the stations in the northern hemisphere mid-latitudes, presumably related to the effect of synoptic scale disturbances, the relatively intense latitudinal mixing and the >8 year lifetime of CH_4.

Furthermore, when the assumed agricultural emissions include a larger ruminant contribution of 10 Tg/y (same as RIC), the RMS deteriorates by -1.9 % and R^2 by +0.3 %.

Note that in this work we focus on the source strengths and neglect inter-annual changes in global OH, which are assumed to be small (Nisbet et al., 2016). Changes in the removal rate of methane by the OH radical have not been seen in other tracers of atmospheric chemistry, e.g. methyl chloroform (CH_3CCl_3) (Montzka et al., 2011; Lelieveld et al. 2016) and do not appear to explain short-term variations in methane. Based on numerical analyses Turner et al. (2017) found that a combination of decreasing methane emissions overlaid by a simultaneous reduction in OH concentration (the primary sink) could have caused the renewed growth in atmospheric methane. However, they could not exclude rising methane emissions under time invariant OH concentrations as a consistent solution to fit the (rising) observations. Changes of the order of 3-5% per year over an 8 year period appear very unlikely.

In the next sections, more detailed analyses are presented to evaluate the emission scenarios.

4.2.1 NOAA and AGAGE stations

The methane emissions scenarios defined above affect Northern- as well as Southern Hemispheric observations. Under the influence of deep convection in the tropics and subsequent global transport, the characteristic seasonality of tropical emissions could significantly influence the CH_4 time series worldwide. Shale gas associated emissions (SHA) from the Northern Hemisphere, however, need a relatively longer time period to influence CH_4 at southern hemispheric stations like South Pole (SPO, 90° S). The agricultural emissions from ruminants (ANI) cover parts of both hemispheres, and the North American SHA emissions are assumed to be seasonally independent. We use the model results together with the measurement data to estimate to which extend possible increases in these tropical and extratropical CH_4 sources can provide a plausible explanation for the observed recent trend.

After introducing the additional a priori emissions of 28 Tg-CH_4/y from 2007 on, the CH_4 increments are calculated at all ground stations for the scenarios TRO, ANI, RIC, and SHA). An obvious overall offset suggests a gross overestimation together with a mismatch in ΔNH/SH, depending on latitudinal source distributions. The latter, compared to the observed 133.84 nmol/mol, varies a priori between 143 (SHA) and 128 (TRO). A suitably downgraded best fit, in the same way as for the no-trend period, can be found by applying the Solver to combinations of the four scenarios. The Solver-optimization procedure suitably reduces the emission amounts for all scenarios to 20.47 Tg CH_4/y on average, in agreement with Kirschke et al. (2013) who suggested 17-22 Tg/y. Small differences between -0.17 and +0.11 are due to varying exposure to OH oxidation. The all-station percentage RMS deviation with 0.44 % indicates a best fit for the RIC scenario, followed by ANI (0.46 %), TRO (0.47 %) and SHA (0.48 %). With ΔNH/SH = 133.76

nmol/mol, RIC optimally fits the interhemispheric difference, whereas TRO with low 128.56 corroborates Schaefer et al. (2016), stating that CH_4 increased mainly in the northern tropics and subtropics. According to Houweling et al. (2014) the TRO input is larger in the southern hemisphere. The match of the observed variability expressed by R^2, with 0.870 is also best for RIC, followed by TRO (0.865), ANI (0.862), and SHA (0.859). All indicators all are comparatively close to each other, however, indications about the role of fossil vs. agricultural emissions, and the latter vs. tropical wetlands, agree with those in the literature based on independent considerations such as $\delta^{13}C$-CH_4 studies (Schaefer at al., 2016). See Table 3 for a summary of all statistical measures.

The optimal combination, with 98 % RIC and 2 % TRO emissions, performs 0.004 % RMS better than RIC alone.

Fig. 10 depicts the CH_4 observations marked by open blue circles at all stations considered from North to South together with the respective no-trend simulations (black crosses) and the Solver-optimized (RIC + TRO) increment (red dots). The respective scatter plots at selected NOAA stations (Fig. 11) indicate good correlation between the observed and calculated station monthly means. NOAA stations records are displayed in Fig. 12, continuing the 1997 through 2006 course (Fig. 5) with optimized (RIC + TRO) increment.

4.2.2 CARIBIC flights

Under the assumptions adopted to explain the station trend, the post-2006 CARIBIC-2 methane measurements appear to be realistically simulated by the EMAC model as well. In Fig. 13 monthly averaged CARIBIC measurements are plotted together with corresponding model results. The slopes of the linear trend lines 0.32x (CARIBIC) and 0.31x (EMAC) over time where x = number of months over the 8 flight observation years 2007 through 2014 (the latest record considered in this study), indicate a very good model representation of the methane trend. The regression analysis with $R^2 = 0.8$ over all flight samples (Fig. 14, upper left panel) even improves for this period, probably also due to a much higher sampling density. As mentioned before, the model underestimates the measured extremes, especially downward excursions observed during northern hemispheric intercontinental flights in April and May 2009, 2011, and 2012 caused by tropopause folds, which at the given vertical grid spacing (~500 m in the UTLS) cannot satisfactorily be resolved by the model. This is confirmed by the frequency spectra (Fig. 15): median simulated values reveal higher amplitudes than measurements before and during the methane-trend period. The different widths of the frequency distributions $\sigma = 6.2$ (EMAC) and 4.7 nmol/mol (CARIBIC) for the period 2007-2014 and $\sigma = 7.4$ and 6.3 nmol/mol, respectively, for the period 2000-2006 confirms the model favoring medium range values.

For detailed comparison with the pre-2007 results, Fig. 16 depicts the whole series on a non-equidistant time axis. Focusing on individual flight sampling regions (Fig. S8) we restrict the statistical analyses (Fig. 14) to areas and periods with at least 300 samples. The highest coefficients of determination ($R^2 > 0.8$) are obtained for NAM, EUR and the FAE. For the other four regions reaching further south such as SAN or IND, the influence of the lower stratosphere is stronger, leading to reduced linear slopes together with comparably less R^2 of 0.59 and 0.72.

4.2.2.1 Selected CARIBIC flights

Individual flights show variations in CH_4 source composition in response to relatively small scale influences. A striking demonstration of the varying influences of emissions in the model in regions crossed by the CARIBIC aircraft is provided by flights 244-245 on August 13–14, 2008, between Frankfurt in Germany and Chennai (formerly Madras) in India. In Fig. 17a (right ordinate) the total observed CH_4 mixing ratios along the flight track are plotted over the respective simulations (with and without trend increment). Typically, simulated peak values are underestimated and not correctly in phase with the observations. Fig. 17b underlines this for the whole collection of India bound CARIBIC

flight samples in accordance with Fig. 15. The post-2006 increment in Fig. 17a (red dashed thick vs red dashed thin) is obvious, but with 1.0 % on average still relatively small in 2008. The source segregated rice paddy-methane (green, left ordinate) dominates the pattern of the total CH_4 and the $R^2 = 0.65$ implies that 0.65 % of the observed CH_4 variability along this special flight track can be explained by rice paddy emissions. Largest mixing ratios in excess of 1,850 nmol/mol were recorded in the upper troposphere between 50° and 75° E. Trajectory calculations as well as methane isotope and other chemical tracer analyses (Schuck et al., 2012; Baker et al., 2012) corroborate that these air masses carry emissions from South and Southeast Asia and can be explained by the trapping of air masses (Rauthe-Schöch et al., 2016) from South Asia in the Upper Troposphere Anticyclone (UTAC), a persistent phenomenon during the monsoon and centered over Pakistan and northern India (Garny and Randel, 2013). This is also qualitatively illustrated in Fig. S9a,b. The methane released by rice paddies in South Asia, trapped in the UTAC, obviously marks the local maximum in the total CH_4 distribution (Fig. S9b - different scales were used for better representation). The flight route crosses this pattern twice, from NW to SE and back. Further, relatively localized maxima in the northern hemispheric extra-tropics (red areas in Fig. S9a) are caused by anthropogenic sources such as coal mining and gas exploitation and from boreal bogs in summer.

Another demonstrative example for tagging results is presented in Fig. S10 which depicts CH_4 mixing-ratios observed during the Far East flight 304 from Osaka, Japan to Frankfurt (Main), Germany in July 2010 together with respective tracers including four of the most relevant individual tagged source contributions. Calculations (red dashed thick, right axis) follow the phase of the measurements (blue dashed, right axis). The trend period increment (the difference between red thick and red thin lines) in 2010 with 1.5 % in average has significantly increased compared to 2008. The pattern is determined by animal-, landfill-, and natural gas source contributions. The determination coefficients with respect to the observations amounts to $R^2 = 0.77$. The pronounced bog-methane profile (color coded in olive-green) dominates the pattern but is not correctly in phase with CARIBIC in terms of an $R^2 = 0.38$. Rice fields east of 136°E contribute relatively strongly.

A more systematic study of the source segregated composition of all 327 CARIBIC flights over the years 1997 through 2014 with special emphasis on the developing trend beyond will be subject of continued investigation.

5 Conclusion and Outlook

We analyzed the atmospheric methane budget by means of EMAC model simulations and comparing the results with data from NOAA and AGAGE surface stations and CARIBIC aircraft data. Source tagging is used to analyze the emission distribution and to optimize the respective amounts in relation to the observations. We found that, compared to our a priory assumptions, a larger natural, biogenic methane source with a concomitant reduction in NH fossil emissions is required to explain the measurements and especially the observed interhemispheric gradient.

Additional methane emission categories such as agriculture, notably rice cultivation (RIC) and ruminant animals (ANI), tropical wetlands (TRO), and North American shale gas extraction (SHA) have been investigated as potential causes of the resuming methane growth since 2007. In agreement with recent literature studies we find that methane increase of 20.45 Tg/y in 2007 and subsequent years, of which 20.02 from RIC and 0.43 from TRO, can optimally explain the trend up to 2013.

We realize that there is no unique solution for the source – receptor relationship. We optimized the size of emissions, the most uncertain aspect of the methane budget, while the – comparably less critical - geographical distribution offers good criteria for optimization, e.g. the interhemispheric difference and the variability.

Therefore, the emissions applied in this work should rather be considered as representative of latitudinal sources than from specific locations. Nevertheless, the degree of freedom in the choice of sources is limited and our scenario realistically represents the north-south gradient of CH_4, being a critical constraint.

In view of the additional global CH_4 source since 2007, a source – sink equilibrium has not yet been established after the 8 years of emissions considered. A 2^{nd} order polynomial exactly fits the course from 2007 through 2013 and the extrapolation predicts steady state after 13 years, assuming that the emissions remain unchanged, which, however, does not seem realistic in view of the observed development after 2013/14 (Fig. 1) and further investigation is needed.

NOAA/AGAGE station data of methane are updated annually so further observational data can be expected. CARIBIC flight measurements have been resumed (after a one-year break). We plan to continue the study of these data, supported with EMAC model simulations, also taking advantage of the most recent and future CARIBIC flights. A larger coverage of Southern Hemispheric sampling routes would be desirable to extend the database and help explain the ongoing, and possibly accelerating upward methane trend.

Acknowledgements:

CARIBIC relevant activities of this modeling project were carried out under contract 320/20585908/IMK-ASF-TOP/GFB by Karlsruhe Institute of Technology (KIT), Karlsruhe.

AGAGE is supported principally by NASA (USA) grants to MIT and SIO, and also by: DECC (UK) and NOAA (USA) grants to Bristol University; CSIRO and BoM (Australia): FOEN grants to Empa (Switzerland); NILU (Norway); SNU (Korea); CMA (China); NIES (Japan); and Urbino University (Italy)

References

Aalst van, M. K., van den Broek, M. M. P., Bregman, A., Brühl, C., Steil, B., Toon, G. C., Garcelon, S., Hansford, G. M., Jones, R. L., Gardiner, T. D., Roelofs, G.-J., Lelieveld, J., and Crutzen, P. J.: Trace gas transport in the 1999/2000 Arctic; comparison of nudged GCM runs with observations, Atmos. Chem. Phys., 4, 81-93, 2004, http://www.atmos-chem-phys.net/4/81/2004/.

Aardenne van J. A. et al.: The EDGAR 3.2 Fast Track 2000 dataset (32FT2000), http://themasites.pbl.nl/tridion/en/themasites/edgar/emission_data/edgar_32ft2000/documentation/index-2.html

Aardenne van J. A., F. J. Dentener, J. G. J. Olivier, J. A. H. W. Peters, and L. N. Ganzeveld (2005), The EDGAR 3.2 fast track 2000 dataset (32FT2000), technical report, Joint Res. Cent., Ispra, Italy. (Available at http://themasites.pbl.nl/tridion/en/themasites/edgar/emission_data/edgar_32ft2000/documentation/index-2.html.)

Baker A., T. J. Schuck, C. A. M. Brenninkmeijer, and Armin Rauthe-Schöch, Estimating the contribution of monsoon-related biogenic production to methane emissions from South Asia using CARIBIC observations, Geophys. Res. Lett., 39, L10813, doi:10.1029/2012GL051756, 2012.

Bergamaschi P., S. Houweling, A. Segers, M. Krol, C. Frankenberg, R. A. Scheepmaker, E. Dlugokencky, S. C. Wofsy, E. A. Kort, C. Sweeney, T. Schuck, C. Brenninkmeijer, H. Chen, V. Beck, and C. Gerbig (2013), AtmosphericCH4 in the first decade of the 21st century: Inverse modeling analysis using SCIAMACHY satellite retrievals and NOAA surface measurements, J. Geophys. Res. Atmos., 118, 7350–7369, doi:10.1002/ jgrd.50480.

Brenninkmeijer C. A. M., Crutzen, P., Boumard, F., Dauer, T., Dix, B., Ebinghaus, R., Filippi, D., Fischer, H., Franke, H., Fries, U., Heintzenberg, J., Helleis, F., Hermann, M., Kock, H. H., Koeppel, C., Lelieveld, J., Leuenberger, M., Martinsson, B. G., Miemczyk, S., Moret, H. P., Nguyen, H. N., Nyfeler, P., Oram, D., O'Sullivan, D., Penkett, S., Platt, U., Pupek, M., Ramonet, M., Randa, B., Reichelt, M., Rhee, T. S., Rohwer, J., Rosenfeld, K., Scharffe, D., Schlager, H., Schumann, U., Slemr, F., Sprung, D., Stock, P., Thaler, R., Valentino, F., van Velthoven, P., Waibel, A., Wandel, A., Waschitschek, K., Wiedensohler, A., Xueref-Remy, I., Zahn, A., Zech, U., and Ziereis, H.: Civil Aircraft for the regular investigation of the atmosphere based on an instrumented container: The new CARIBIC system, Atmos. Chem. Phys., 7, 4953-4976, doi:10.5194/acp-7-4953-2007, 2007.

Brenninkmeijer C.A.M. , P. J. Crutzen , H. Fischer , H. Güsten , W. Hans , G. Heinrich , J. Heintzenberg , M. Hermann, T. Immelmann , D. Kersting , M. Maiss , M. Nolle , A. Pitscheider , H. Pohlkamp , D. Scharffe , K. Specht , and A. Wiedensohler , 2010: CARIBIC-Civil Aircraft for Global Measurement of Trace Gases and Aerosols in the Tropopause Region. Journal of Atmospheric and Oceanic Technology, 16, 1373-1383, doi: 10.1175/1520-0426(1999)

Brenninkmeijer C.A.M. , P. J. Crutzen, F. Boumard, T. Dauer, B. Dix, R. Ebinghaus, D. Filippi, H. Fischer, H. Franke, U. Frieß, J. Heintzenberg, F. Helleis, M. Hermann, H. H. Kock, C. Koeppel, J. Lelieveld, M. Leuenberger, B. G. Martinsson, S. Miemczyk, H. P. Moret, H. N. Nguyen, P. Nyfeler, D. Oram, D. O'Sullivan, S. Penkett, U. Platt, M. Pupek, M. Ramonet, B. Randa, M. Reichelt, T. S. Rhee, J. Rohwer, K. Rosenfeld, D. Scharffe, H. Schlager, U. Schumann, F. Šlemr, D. Sprung, P. Stock, R. Thaler, F. Valentino, P. van Velthoven, A. Waibel, A. Wandel, K. Waschitschek, A. Wiedensohler, I. Xueref-Remy, A. Zahn, U. Zech, and H. Ziereis, Civil Aircraft for the Regular Investigation of the atmosphere Based on an Instrumented Container: The new CARIBIC system. Atmospheric Chemistry and Physics (ACP) 2007

Ciais, P., C. Sabine, G. Bala, L. Bopp, V. Brovkin, J. Canadell, A. Chhabra, R. DeFries, J. Galloway, M. Heimann, C. Jones, C. Le Quéré, R.B. Myneni, S. Piao and P. Thornton, 2013: Carbon and Other Biogeochemical Cycles. In: Climate Change 2013: The Physical Science Basis. Contribution of Working Group I to the Fifth Assessment Report of the Intergovernmental Panel on Climate Change [Stocker, T.F., D. Qin, G.-K. Plattner, M. Tignor, S.K. Allen, J. Boschung, A. Nauels, Y. Xia, V. Bex and P.M. Midgley (eds.)]. Cambridge University Press, Cambridge, United Kingdom and New York, NY, USA.

Crutzen P. J.: The " anthropocene ", J. Phys. IV France 12 (2002), DOI : 10. 1051/j:p2 40 020447

Cunnold D.M., L.P. Steele, P.J. Fraser, P.G. Simmonds, R.G. Prinn, R.F. Weiss, L.W. Porter, R.L. Langenfelds, H.J. Wang, L. Emmons, X.X. Tie, and E.J. Dlugokencky, In situ measurements of atmospheric methane at GAGE/AGAGE sites during 1985-2000 and resulting source inferences. J. Geophys. Res., 107, D14, doi: 10.1029/2001JD001226, 2002.

Curry C. L. (2007), Modeling the soil consumption of atmospheric methane at the global scale, Global Biogeochem. Cycles, 21, GB4012, doi:10.1029/2006GB002818.

Dee, D. P., Uppala, S. M., Simmons, A. J., Berrisford, P., Poli, P., Kobayashi, S., Andrae, U., Balmaseda, M. A., Balsamo, G., Bauer, P., Bechtold, P., Beljaars, A. C. M., van de Berg, L., Bid-lot, J., Bormann, N., Delsol, C., Dragani, R., Fuentes, M., Geer, A. J., Haimberger, L., Healy, S. B., Hersbach, H., Hólm, E. V., Isaksen, L., Kållberg, P., Köhler, M., Matricardi, M., McNally, A. P., Monge-Sanz, B. M., Morcrette, J.-J., Park, B.-K., Peubey, C., de Rosnay, P., Tavolato, C., Thépaut, J.-N., and Vitart, F.: The ERA-Interim reanalysis: configuration and performance of the data assimilation system, Q. J. Roy. Meteor. Soc., 137, 553–597, doi:10.1002/qj.828, 2011.

Dentener F., Kinne, S., Bond, T., Boucher, O., Cofala, J., Generoso, S., Ginoux, P., Gong, S., Hoelzemann, J. J., Ito, A., Marelli, L., Penner, J. E., Putaud, J.-P., Textor, C., Schulz, M., van der Werf, G. R., and Wilson, J.: Emissions of primary aerosol and precursor gases in the years 2000 and 1750 prescribed data-sets for AeroCom, Atmos. Chem. Phys., 6, 4321-4344, doi:10.5194/acp-6-4321-2006, 2006.

Dlugokencky, E. J., R. C. Myers, P. M. Lang, K. A. Masarie, A. M. Crotwell, K. W. Thoning, B. D. Hall, J. W. Elkins, and L. P. Steele (2005), Conversion of NOAA atmospheric dry air CH4 mole fractions to a gravimetrically prepared standard scale, J. Geophys. Res., 110, D18306, doi:10.1029/2005JD006035.

Dlugokencky, E. J., L. Bruhwiler, J. W. C. White, L. K. Emmons, P. C. Novelli, S. A. Montzka, K. A. Masarie, P. M. Lang, A. M. Crotwell, J. B. Miller, and L. V. Gatti, Observational constraints on recent increases in the atmospheric CH4 burden, Geophys. Res. Lett., 36(L18803), doi: 10.1029/2009GL039780, 2009.

Dlugokencky, E. J., E. G. Nisbet, R. Fisher, and D. Lowry, Global atmospheric methane: budget, changes and dangers, Phil. Trans. R. Soc. A 369(1943), 2058-2072, doi: 10.1098/rsta.2010.0341, 2011.

Dlugokencky, E.J., P.M. Lang, A.M. Crotwell, J.W. Mund, M.J. Crotwell, and K.W. Thoning (2018), Atmospheric Methane Dry Air Mole Fractions from the NOAA ESRL Carbon Cycle Cooperative Global Air Sampling Network, 1983-2017, Version: 2018-08-01, Path: ftp://aftp.cmdl.noaa.gov/data/trace_gases/ch4/flask/surface/.

Etminan, M., G. Myhre, E. J. Highwood, and K. P. Shine (2016), Radiative forcing of carbon dioxide, methane, and nitrous oxide: A significant revision of the methane radiative forcing, Geophys. Res. Lett., 43, 12,614 – 12,623, doi:10.1002/2016GL071930.

Frank, F. I.: Atmospheric methane and its isotopic composition in a changing climate, Ph.D. thesis, Ludwig-Maximilians-Universität, München, URL http://nbn-resolving.de/urn:nbn:de:bvb:19-225789 (2018)

FAO, 2010: http://foris.fao.org/static/data/fra2010/StateofForests_Report_English.pdf

Forster P. et al. 2007 Changes in atmospheric constituents and in radiative forcing. In Climate change 2007: the physical science basis. Contribution of Working Group I to the Fourth Assessment Report of the Intergovernmental Panel on Climate Change (eds S. Solomon, D. Qin, M. Manning, Z. Chen, M. Marquis, K. Averyt, M. Tignor & H. Miller). Cambridge, UK: Cambridge University Press.

FracFocus, 2016, The national hydraulic fracturing chemical registry, http://fracfocus.org/

Fung, I., J. John, J. Lerner, E. Matthews, M. Prather, L. P. Steele, and P .J. Fraser, Three-dimensional model synthesis of the global methane cycle, J. Geophys. Res., 96, 13,033-13,065, 1991.

Garny, H., and W. J. Randel (2013), Dynamic variability of the Asian monsoon anticyclone observed in potential vorticity and correlations with tracer distributions, J. Geophys. Res. Atmos., 118, 13,421–13,433, doi:10.1002/2013JD020908.

Helmig, D., Rossabi, S., Hueber, J., Tans, P., Montzka, S.A., Masarie, K., Thoning,K., Plass-Duelmer, C., Claude, A., Carpenter, L.J., Lewis, A.C., Punjabi, S., Reimann, S., Vollmer, M.K., Steinbrecher, R., Hannigan, J.W., Emmons, L.K., Mahieu, E., Franco, B., Smale, D. and Pozzer, A. : Reversal of global atmospheric ethane and propane trends largely due to US oil and natural gas production", Nature Geoscience, 9, 490-495, doi:10.1038/ngeo2721, 2016

Houweling S., F. J. Dentener, J. Lelieveld, B. Walter, and E. J. Dlugokencky (2000b), The modeling of tropospheric methane: How well can point measurements be reproduced by a global model?, J. Geophys. Res., 105, 8981- 9002

Houweling S., T. Röckmann, I. Aben, F. Keppler, M. Krol, J. F. Meirink, E. J. Dlugokencky, and C. Frankenberg (2006), Atmospheric constraints on global emissions of methane from plants, Geophys. Res. Lett., 33, L15821, doi:10.1029/2006GL026162.

IPCC, 2013: Summary for Policymakers. In: Climate Change 2013: The Physical Science Basis. Contribution of Working Group I to the Fifth Assessment Report of the Intergovernmental Panel on Climate Change [Stocker, T.F., D. Qin, G.-K. Plattner, M. Tignor, S.K. Allen, J. Boschung, A. Nauels, Y. Xia, V. Bex and P.M. Midgley (eds.)], Cambridge University Press, Cambridge, United Kingdom and New York, NY, USA.

IPCC, 2014: Climate Change 2014: Synthesis Report. Contribution of Working Groups I, II and III to the Fifth Assessment Report of the Intergovernmental Panel on Climate Change [Core Writing Team, R.K. Pachauri and L.A. Meyer (eds.)]. IPCC, Geneva, Switzerland, 151 pp.

Jöckel P., A. Kerkweg, A. Pozzer, R. Sander, H. Tost, H. Riede, A. Baumgaertner, S. Gromov, and B. Kern, Development cycle 2 of the Modular Earth Submodel System (MESSy2), Geosci. Model Dev., 3, 717-752, doi:10.5194/gmd-3-717-2010, 2010

Jöckel P., Tost, H., Pozzer, A., Brühl, C., Buchholz, J., Ganzeveld, L., Hoor, P., Kerkweg, A., Lawrence, M. G., Sander, R., Steil, B., Stiller, G., Tanarhte, M., Taraborrelli, D., van Aardenne, J., and Lelieveld, J.: The atmospheric chemistry general circulation model ECHAM5/MESSy1: consistent simulation of ozone from the surface to the mesosphere, Atmos. Chem. Phys., 6, 5067- 5104, doi:10.5194/acp-6-5067-2006, 2006.

Kai F.M, Stanley C. Tyler, J.T. Randerson, and D.R. Blake, Reduced methane growth rate explained by decreased Northern Hemisphere microbial sources, Nature 476, 194–197, 2011, doi:10.1038/nature10259.

Karion A., et al. (2013), Methane emissions estimate from airborne measurements over a western United States natural gas field, Geophys. Res. Lett., 40, 4393-4397, doi:10.1002/grl.50811.

Kerkweg, A., Buchholz, J., Ganzeveld, L., Pozzer, A., Tost, H., and Jöckel, P.: Technical Note: An implementation of the dry removal processes DRY DEPosition and SEDImentation in the Modular Earth Submodel System (MESSy), Atmos. Chem. Phys., 6, 4617-4632, https://doi.org/10.5194/acp-6-4617-2006, 2006.

Krol, M., de Bruine, M., Killaars, L., Ouwersloot, H., Pozzer, A., Yin, Y., Chevallier, F., Bousquet, P., Patra, P., Belikov, D., Maksyutov, S., Dhomse, S., Feng, W., and Chipperfield, M. P.: Age of Air as a diagnostic for transport time-scales in global models, Geosci. Model Dev. Discuss., https://doi.org/10.5194/gmd-2017-262, 2017.

Lelieveld J., P. J. Crutzen, and F. J. Dentener, Changing concentration, lifetime and climate forcing of atmospheric methane, Tellus, 50B, 128-150, 1998.

Lelieveld, J., S. Gromov, A. Pozzer, and D. Taraborrelli, Global tropospheric hydroxyl distribution, budget and reactivity, Atmos. Chem. Phys., 16, 12477-12493, 2016.

Mikaloff-Fletcher, Sara E. and Schaefer H., Rising methane: A new climate challenge, Science 364 (6444), 932-933, DOI: 10.1126/science.aax1828, 2019.

Montzka, S., M. Krol, E. Dlugokencky, B. Hall, P. Jöckel, and J. Lelieveld, Small inter-annual variability of global atmospheric hydroxyl, Science, 331, 67-69, 2011.

Nisbet, E. G., et al. (2016): Rising atmospheric methane: 2007–2014 growth and isotopic shift, Global Biogeochem. Cycles, 30, 1356–1370, doi:10.1002/2016GB005406.

Olivier Jos G.J. , Jan J.M. Berdowski, Jeroen A.H.W. Peters, Joost Bakker, Antoon J.H. Visschedijk and JanPieter J. Bloos, Applications of EDGAR, RIVM report 773301001 / NRP report 410 200 051, 2001/2002

Prinn, R. G., R.F. Weiss, P.B. Krummel, S. O'Doherty, P.J. Fraser, J. Muhle, S. Reimann, M.K. Vollmer, P.G. Simmonds, M. Maione, J. Arduini, C.R. Lunder, N. Schmidbauer, D. Young, H.J. Wang, J. Huang, M. Rigby, C.M. Harth, P.K. Salameh, T.G Spain, L.P. Steele, T. Arnold, J. Kim, O. Hermansen, N. Derek, B. Mitrevski, and R. Langenfelds (2016), The ALE / GAGE AGAGE Network, Carbon Dioxide Information Analysis Center (CDIAC), Oak Ridge National Laboratory (ORNL), U.S. Department of Energy (DOE).

Prinn R. G., R.F. Weiss, P. J. Fraser, P. G. Simmonds, D. M. Cunnold, S. O'Doherty, P. K. Salameh, L. W. Porter, P. B. Krummel, R. H. J. Wang, B. R. Miller, C. Harth, B. R. Greally, F. A. Van Woy, L. P. Steele, J. Mühle, G. A. Sturrock, F. N. Alyea, J. Huang, and D. E. Hartley (2013), The ALE / GAGE AGAGE Network, Carbon Dioxide Information Analysis Center (CDIAC), Oak Ridge National Laboratory (ORNL), U.S. Department of Energy (DOE).

Prinn R. G., R.F. Weiss, P. J. Fraser, P.G. Simmonds, D.M. Cunnold, F.N. Alyea, S. O'Doherty, P. Salameh, B.R. Miller, J. Huang, R.H.J. Wang, D.E. Hartley, C. Harth, L.P. Steele, G. Sturrock, P.M. Midgley, and A. McCulloch, A History of Chemically and Radiatively Important Gases in Air deduced from ALE/GAGE/AGAGE, J. Geophys. Res., 105, 17,751- 17,792, 2000

Prinn R. G., et al., "The ALE/GAGE/AGAGE network." carbon (1978).

Randerson, J. T., G.R. van der Werf, L. Giglio, G.J. Collatz, and P.S. Kasibhatla. 2018. Global Fire Emissions Database, Version 4, (GFEDv4). ORNL DAAC, Oak Ridge, Tennessee, USA. https://doi.org/10.3334/ORNLDAAC/1293

Rauthe-Schöch A., Baker A. K., Schuck T.J., Brenninkmeijer C.A.M., Zahn A., Hermann M., Stratmann G., Ziereis H., van Velthoven P.F.J., and Lelieveld J.: Trapping, chemistry and export of trace gases in the South Asian summer monsoon observed during CARIBIC flights in 2008, Atmos. Chem. Phys., 16, 3609-3629, doi:10.5194/acp-16-3609-2016, 2016.

Rigby, M., R. G. Prinn, P. J. Fraser, P. G. Simmonds, R. L. Langenfelds, J. Huang, D. M. Cunnold, L. P. Steele, P. B. Krummel, R. F. Weiss, S. O'Doherty, P. K. Salameh, H. J. Wang, C. M. Harth, J. Mühle, and L. W. Porter, Renewed growth of atmospheric methane, Geophys. Res. Lett., 35(L22805), doi:10.1029/2008GL036037, 2008.

Rigby, M., S. A. Montzka, R. G. Prinn, J. W. C. White, D. Young, S. O'Doherty, M. F. Lunt, A. L. Ganesan, A. J. Manning, P. G. Simmonds, P. K. Salameh, C. M. Harth, J. Mühle, R. F. Weiss, P. J. Fraser, L. P. Steele, P. B. Krummel, A. McCulloch, and S. Park, Role of atmospheric oxidation in recent methane growth, Proceedings of the National Academy of Sciences, 114(21), 5373-5377, doi: 10.1073/pnas.1616426114, 2017.

Roeckner E. et al., Sensitivity of simulated climate to horizontal and vertical resolution in the ECHAM5 atmosphere model, J. Climate, 19, 3771-3791, 2006.

Schaefer, H. et al. A 21st century shift from fossil-fuel to biogenic methane emissions indicated by $^{13}CH_4$. Science 352, 80–84 (2016).

Schuck T. J., K. Ishijima, P. K. Patra, A. K. Baker, T. Machida, H. Matsueda, Y. Sawa, T. Umezawa, C. A. M. Brenninkmeijer, and J. Lelieveld (2012), Distribution of methane in the tropical upper troposphere measured by CARIBIC and CONTRAIL aircraft, J. Geophys. Res., 117, D19304, doi:10.1029/2012JD018199.

Simpson, I.J. et al., Long-term decline of global atmospheric ethane concentrations and implications for methane, Nature 488, 490–494 (2012), doi:10.1038/nature11342

Spahni R. et al., Constraining global methane emissions and uptake by ecosystems, Biogeosciences, 8, 1643-1665, doi:10.5194/bg-8-1643-2011, 2011

Saunois M. et al., The global methane budget 2000–2012, Earth System Science Data, 8 (2). pp. 697-751. ISSN 1866-3508, 2016.

Turner, A. J., D. J. Jacob, J. Benmergui, S. C. Wofsy, J. D. Maasakkers, A. Butz, O. Hasekamp, and S. C. Biraud (2016), A large increase in U.S. methane emissions over the past decade inferred from satellite data and surface observations, *Geophys. Res. Lett.*, *43*, 2218–2224, doi:10.1002/2016GL067987.

Turner, A. J., C. Frankenberg, P. O.Wennberg, and D. J. Jacob, Ambiguity in the causes for decadal trends in atmospheric methane and hydroxyl, Proceedings of the National Academy of Sciences, 114(21), 5367-5372, doi: 10.1073/pnas.1616020114, 2017.

Worden, J. R., A. A. Bloom, S. Pandey, Z. Jiang, H. M. Worden, T. W. Walker, S.

Walter B. and Heimann M., A process-based climate-sensitive model to derive methane emissions from natural wetlands: Application to five wetland sites, sensitivity to model parameters, and climate, GLOBAL BIOGEOCHEMICAL CYCLES, VOL. 14, NO. 3, PAGES 745-765, SEPTEMBER 2000

White J.W.C., B.H. Vaughn, and S.E. Michel (2015), University of Colorado, Institute of Arctic and Alpine Research (INSTAAR), Stable Isotopic Composition of Atmospheric Methane (13C) from the NOAA ESRL Carbon Cycle Cooperative Global Air Sampling Network, 1998-2014, Version: 2016-04-26, Path: http://aftp.cmdl.noaa.gov/data/trace_gases/ch4c13/flask/.

Worden, J. R., A. A. Bloom, S. Pandey, Z. Jiang, H. M. Worden, T. W. Walker, S. Houweling, and T. Röckmann, Reduced biomass burning emissions reconcile conflicting estimates of the post-2006 atmospheric methane budget, Nature Communications, 8(1), 2227, doi: 10.1038/s41467-017-02246-0, 2017.

Acronyms:

EMAC	ECHAM/MESSy Atmospheric Chemistry (EMAC) model
ECHAM	European Center for medium range weather forecast operational model HAMburg version
GAIM	GLOBAL ANALYSIS,INTEGRATION, AND MODELLING
IGBP	International Geosphere-Biosphere Programme
EDGAR	Emissions Database for Global Atmospheric Research
GFED	Global Fire Emissions Database
AGAGE	Advanced Global Atmospheric Gases Experiment
NOAA	National Oceanic and Atmospheric Administration

Code	Station Name	Country	Lat °	Lon °	elevation / m
ALT	Alert	Canada	82.45	-62.51	190
ASC	Ascension Island	UK	-7.97	-14.40	85
AZR	Terceira Ile., Azores	Portugal	38.77	-27.38	19
BRW	Barrow, Alaska	USA	71.32	-156.61	11
CGO	Cape Grim, Tasmania	Australia	-40.68	144.69	94
CRZ	Crozet Island	France	-46.43	51.85	197
EIC	Easter Island	Chile	-27.16	-109.43	47
GMI	Mariana Islands	Guam	13.39	144.66	0
HBA	Halley Station,	Antarctica, UK	-75.61	-26.21	30
MLO	Mauna Loa, Hawaii	USA	19.54	-155.58	3397
RPB	Ragged Point	Barbados	13.17	-59.43	15
SEY	Mahe Island,	Seychelles	-4.68	55.53	2
SHM	Shemya Island, Alaska	USA	52.71	174.13	23
SMO	Tutuila, Am. Samoa	USA	-14.25	-170.56	42
SPO	South Pole	USA	-89.98	-24.80	2810
ZEP	Ny-Alesund, Svalbard	Norway, Sweden	78.91	11.89	474

CARIBIC	Civil Aircraft for the Regular observation of the atmosphere Based on an Instrumented Container
AFR	Africa
EUR	Europe
FAE	Far East
IND	India
NAM	North America
SAN	South America north
SAS	South America south

Rising methane emission scenarios 2007-2013:

TRO	Tropical wetland
SHA	Shale gas production
RIC	Rice cultivation
ANI	Ruminant Animals
ITCZ	Inter-Tropical Convergence Zone

Tables

CH_4 sources		emission Tg (CH_4)/y		lifetime [y]	Seasonality
Code	**category**	**a priory** [1)]	**final** [6)]		
swa	swamps	133	140	10.08	yes
ani	animals	98	100	8.18	
lan	landfills	68	65	7.25	
ric	rice paddies	60	64	7.79	yes
gas	gas production	48	42	7.86	
bog	bogs	42	40	8.91	yes
coa	coal mining	42	31	9.20	
	oceans + offshore traffic [2)]	17			
	oil production, processing [2)]	8			
	other anthrop. Sources [2,3)]	6			
	volcanoes [2)]	4			
oil	oil related	35	33	7.37	
bib	biomass burning [4)]	20	25	-	yes
ter	termites	19	20	7.94	
bfc	biofuel combustion[5)]	15	16	7.88	
	sum	**580**	**577**	8.45	yes

Table 1:

[1)] Methane emissions (Houweling et al. 2006) for EMAC model input 1997 – 2006 (no-trend period).

[2)] merged in one category "oil related" by [1)]

[3)] all EDGAR emission classes related to the use of fossil fuels such as residential heating, onshore traffic, industry,

[4)] *GFEDv4s statistics (Randerson et al., 2018)*

[5)] *EDGAR2.0 database (Olivier, 2001).*

[6)] rescaled with respect to minimal station observation to model simulation RMS.

	Flight region:	Europe	Africa	Far East	India	North America	South Am. north	South Am. South	Globe
	Acronym:	EUR	AFR	FAE	IND	NAM	SAN	SAS	ALL
					No-trend period mean 1997-2006:				
C1	**observations**	1.783E-06	1.781E-06	1.793E-06	1.788E-06	no flights	1.786E-06	1.778E-06	1.786E-06
C2	**model**	1.790E-06	1.783E-06	1.792E-06	1.793E-06		1.785E-06	1.777E-06	1.788E-06
C3	**RMS %**	1.23	0.69	1.24	0.80		0.75	0.76	1.01
C4	**R^2**	0.82	0.43	0.62	0.67		0.60	0.64	0.65
C5	**samples %**	18.1	4.7	21.5	31.5	0.0	10.5	13.6	100.00
					Trend phase mean 2007-2014:				
T1	**observations**	1.791E-06	1.802E-06	1.802E-06	1.811E-06	1.773E-06	1.813E-06	1.839E-06	1.801E-06
T2	**model**	1.796E-06	1.796E-06	1.805E-06	1.806E-06	1.785E-06	1.804E-06	1.818E-06	1.800E-06
T3	**RMS %**	1.40	1.08	1.44	1.04	1.70	1.03	1.44	1.31
T4	**R^2**	0.84	0.58	0.81	0.72	0.84	0.59	0.29	0.80
T5	**samples %**	25.7	6.9	20.4	8.7	10.3	24.6	3.5	100

Table 2: Statistical evaluation of CARIBIC flight methane samples versus EMAC model simulations based on optimized emissions.

Scenarios:	TG/y	RMS %	R^2	Δ NH/SH[1)]
RIC	20.44	0.44	0.8697	133.76
ANI	20.64	0.46	0.8620	134.88
TRO	20.51	0.47	0.8654	128.57
SHA	20.36	0.48	0.8588	139.17
observations				*133.84*

[1)] Difference between most northern and southern stations

Table 3: Statistical evaluation of rising-methane scenarios – best match underlined.

Figures

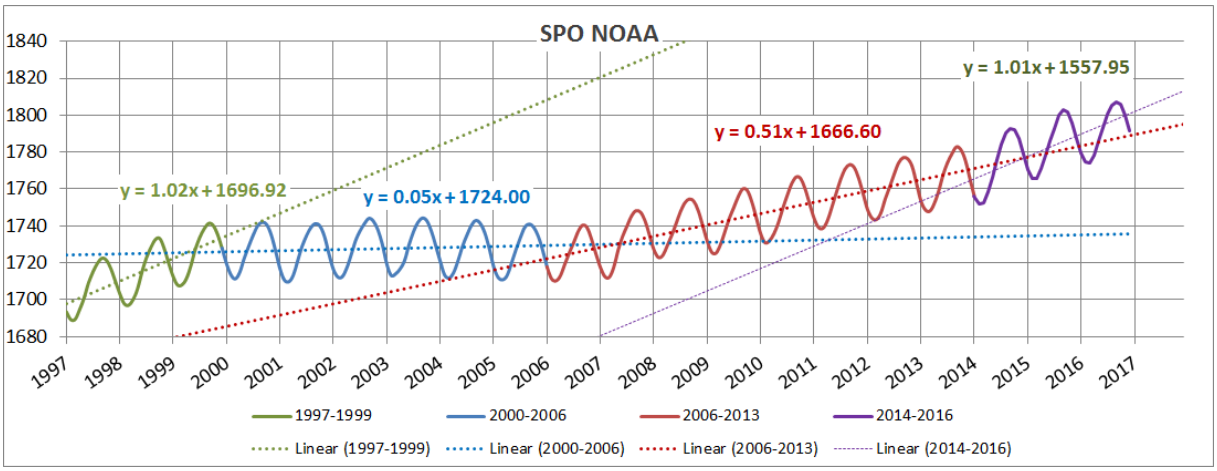

Figure 1: Development of monthly mean CH_4 mixing- ratios at the NOAA observation site South Pole (SPO, 90° S) over the years 1997 through 2016, the period considered in this modeling study.

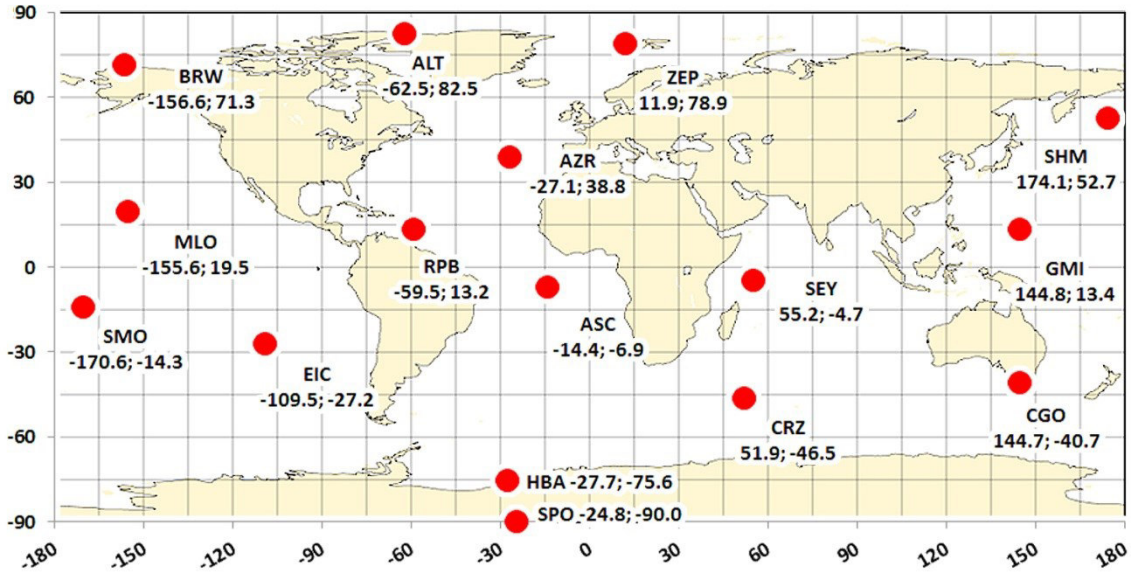

Figure 2a: Map of NOAA sampling locations for greenhouse gases used for reference in this study (see Table 1 for names and coordinates).

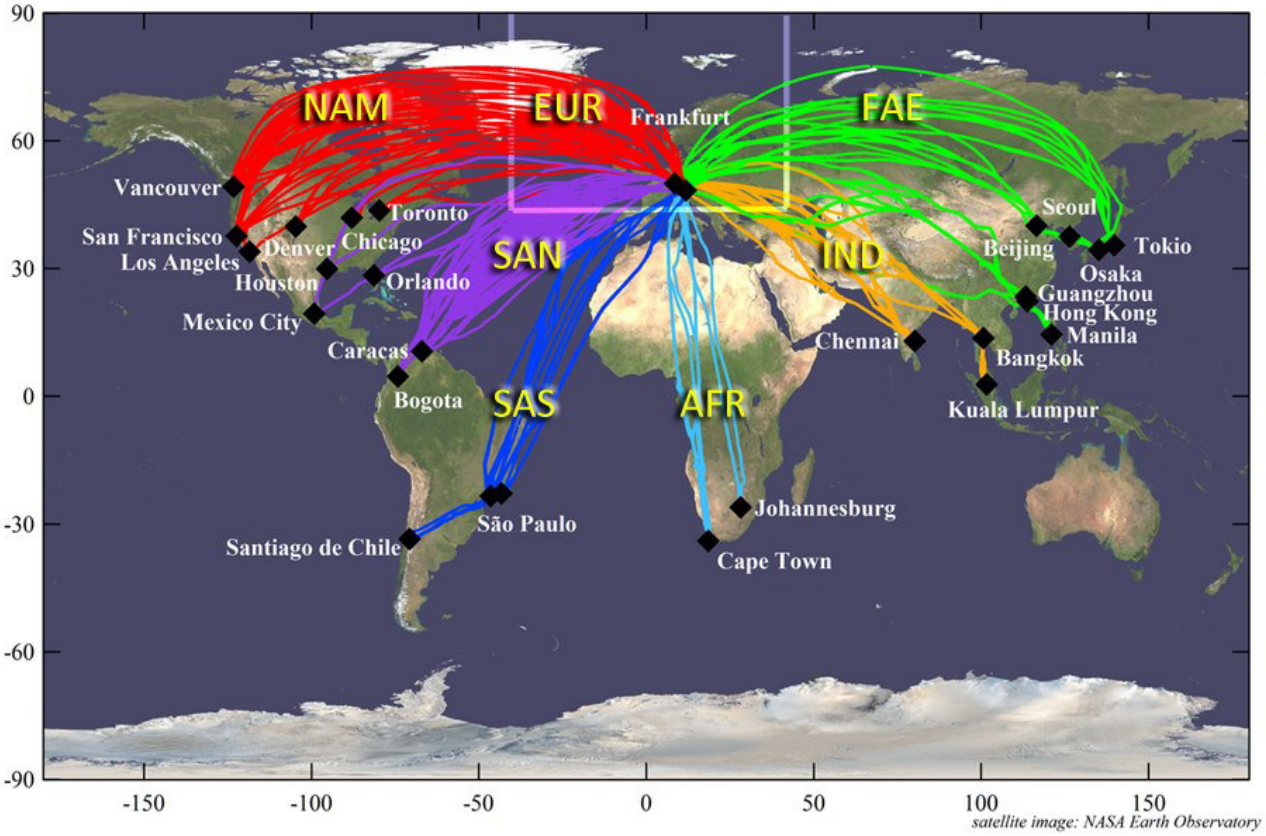

b: CARIBIC flights and destinations

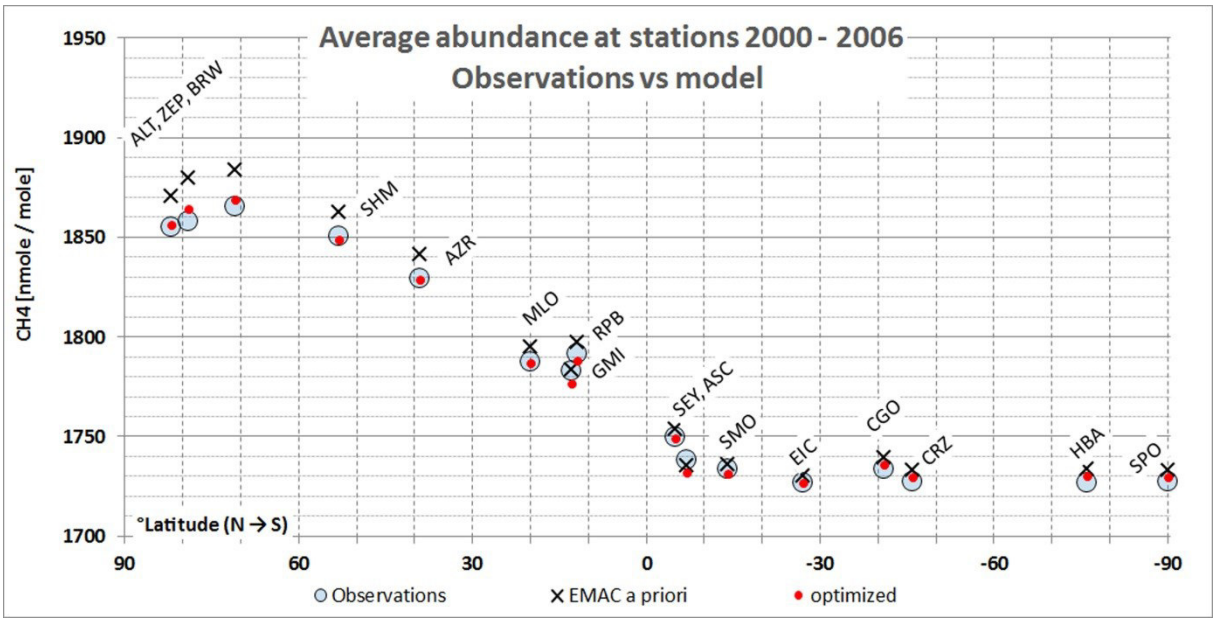

Figure 3: Optimization of calculated ground station CH_4 mixing-ratios towards observations (blue circles): A priori simulations (black crosses) - a posteriori simulations (red dots).

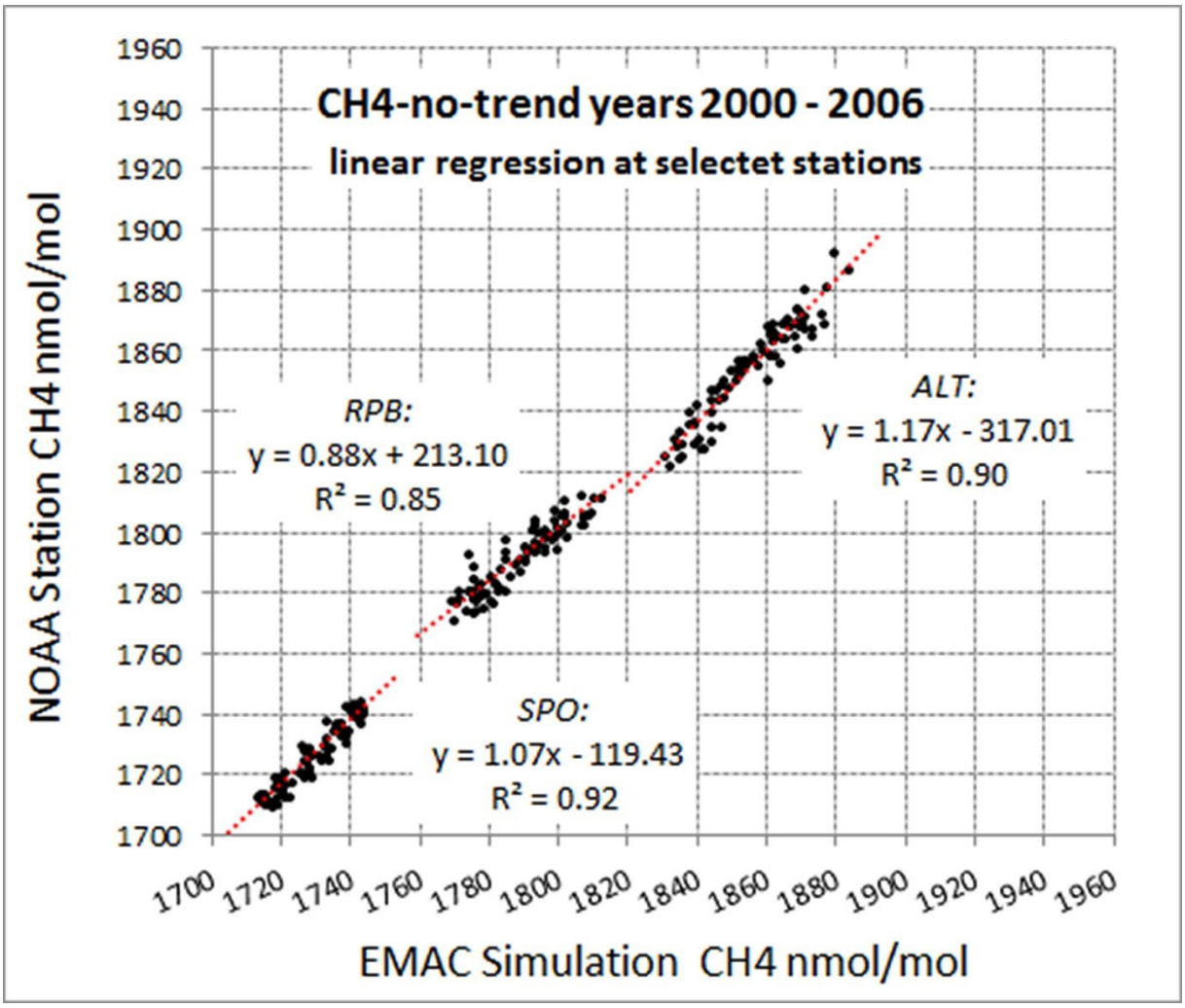

Figure 4: Regression analysis of EMAC calculations vs. observations of CH_4 at NOAA stations ALT, RPB, and SPO for no-trend years 2000 through 2006.

30

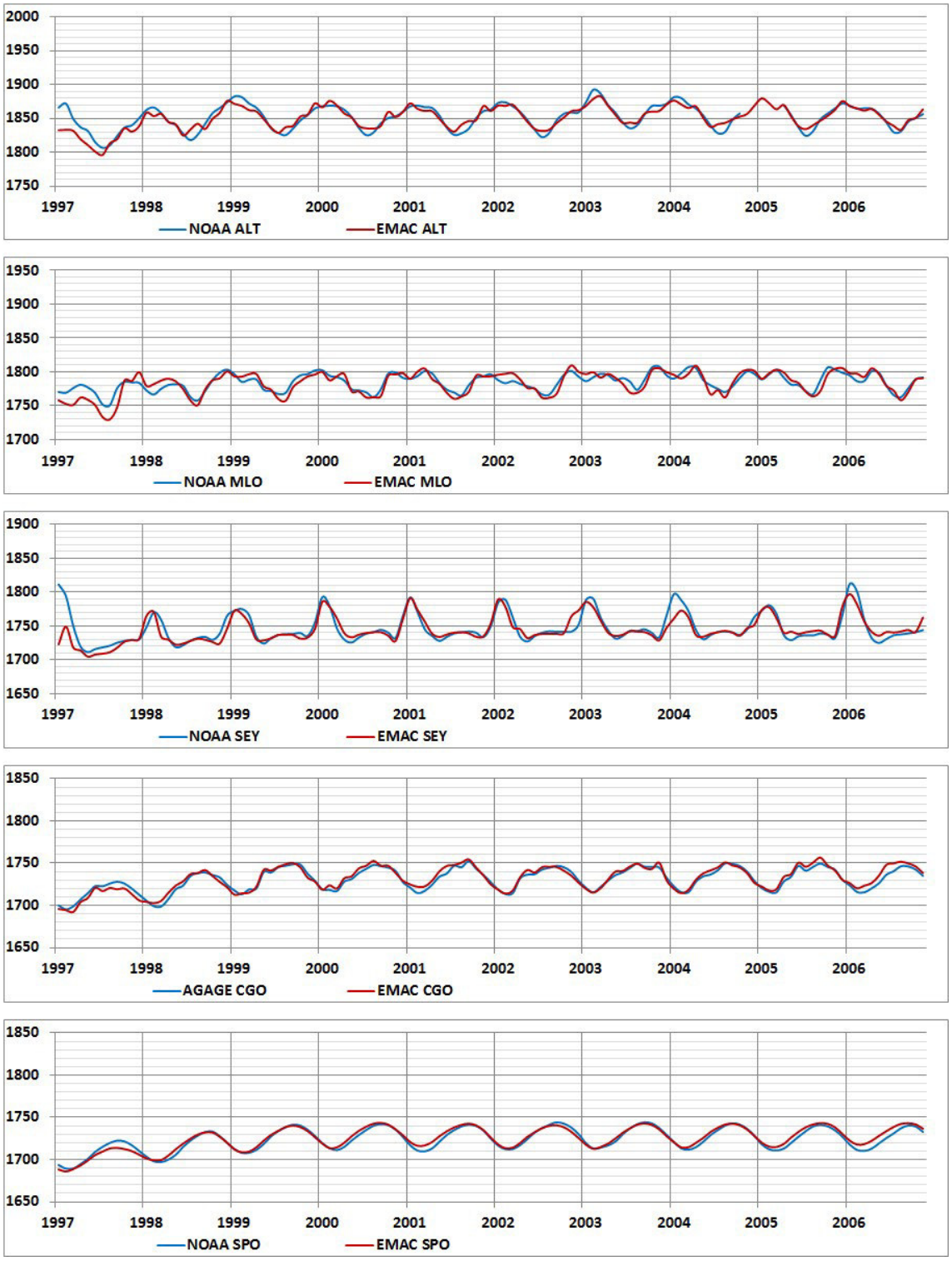

Figure 5: EMAC calculations (red) vs NOAA and AGAGE observations (blue) of CH_4 from 1997 through 2006.

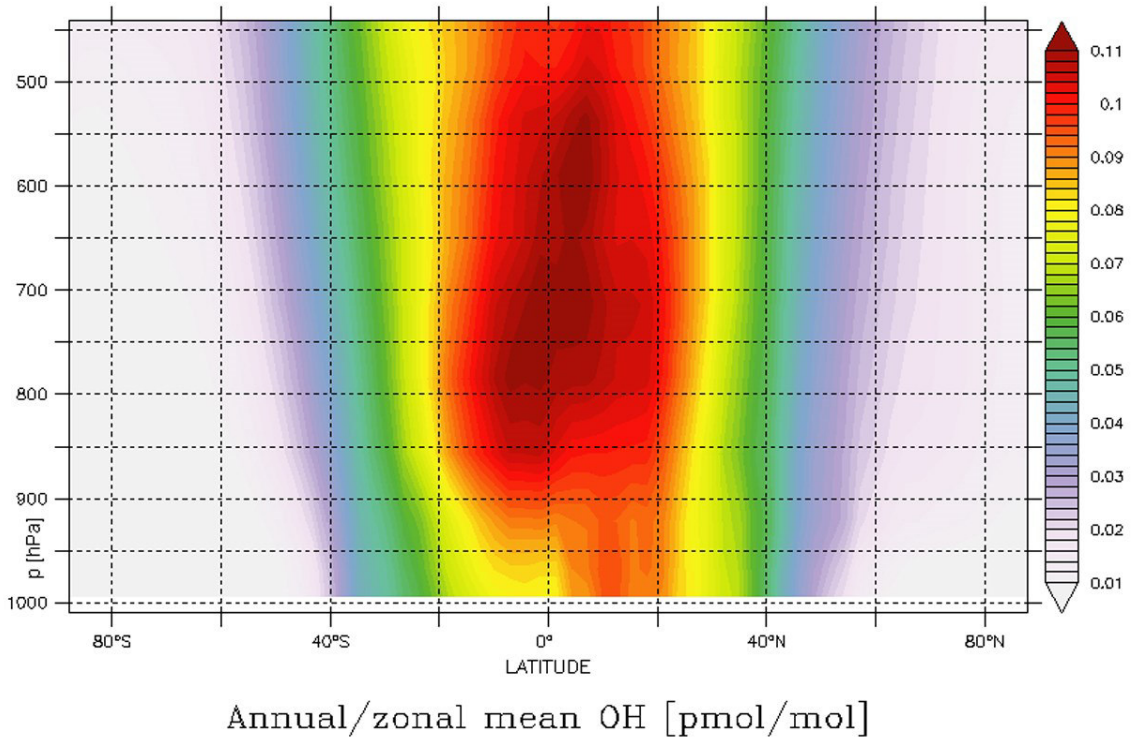

Figure 6: In the Northern Hemisphere lower troposphere the OH mixing-ratios are considerably higher than on the Southern Hemisphere

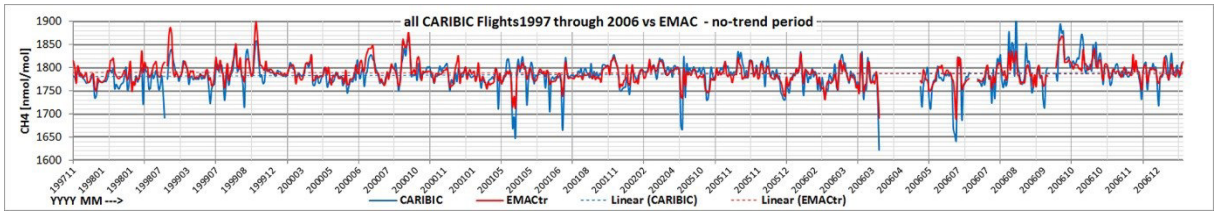

Figure 7:

EMAC CH_4 calculations (red) and CARIBIC-1/2 observations (blue) from 1997 through 2006 – all flight samples.

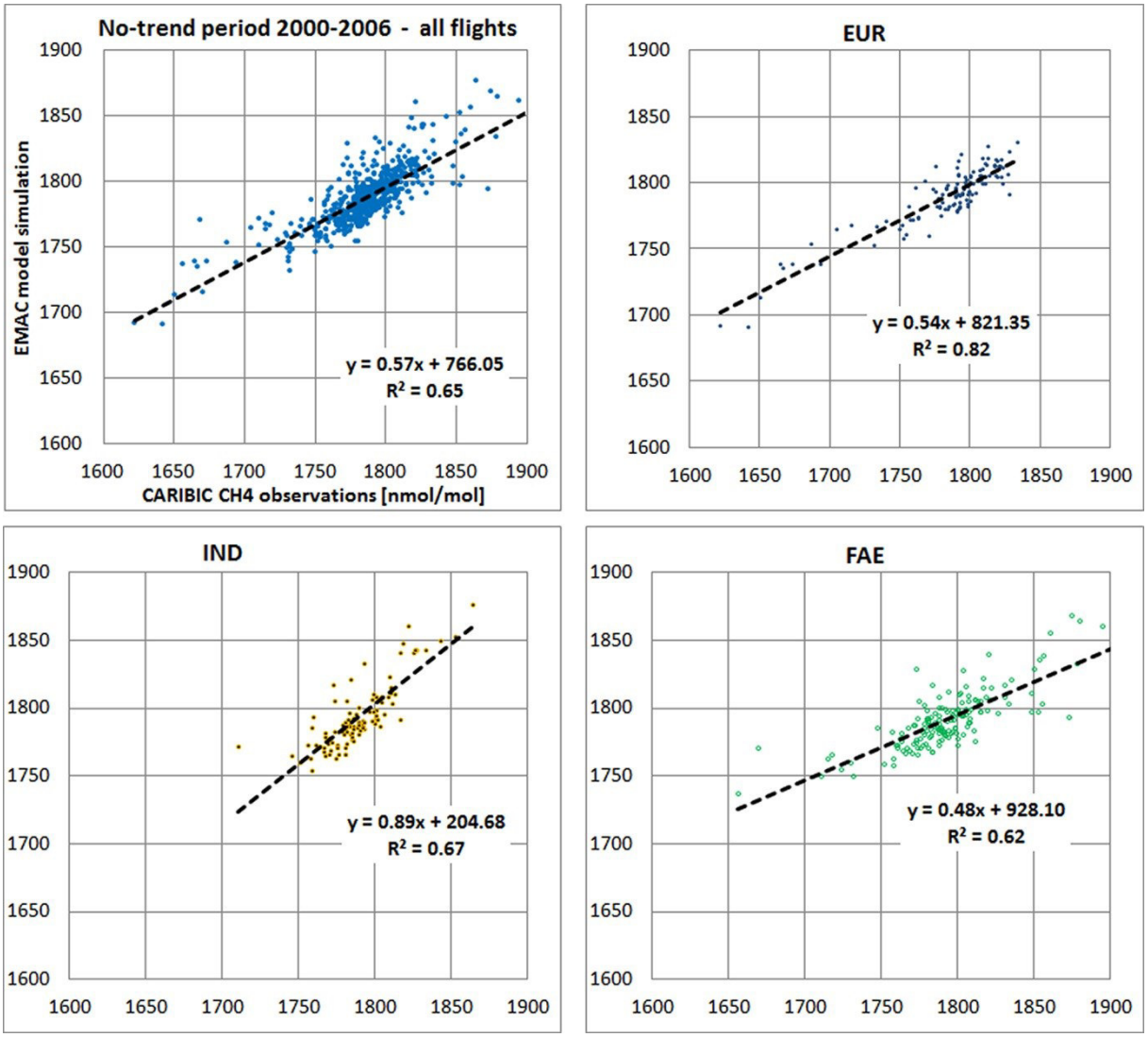

Figure 8: Correlation EMAC vs. CARIBIC flights, 2000 - 2006 (no-trend period).

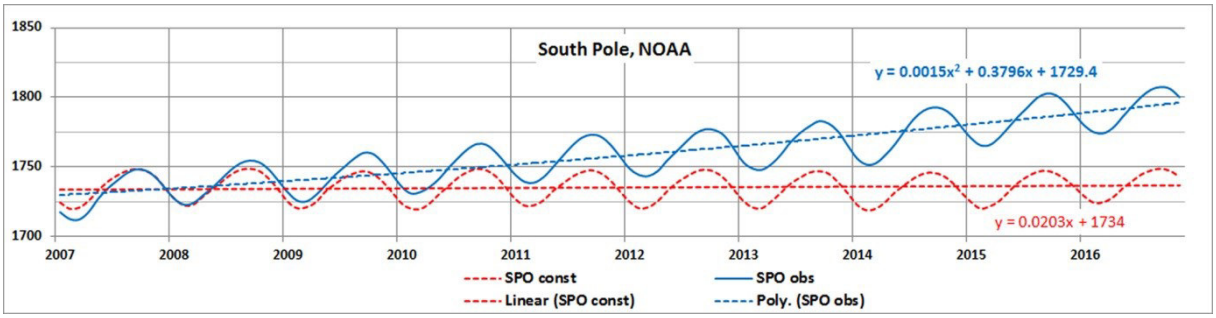

Figure 9:

a: NOAA observations at the South Pole (blue) from 2007 through 2016 compared to EMAC CH_4 calculations (red) under 1997-2006 unchanged emission assumption. The observed trend is no longer linear and increasing after 2013 (dashed blue)

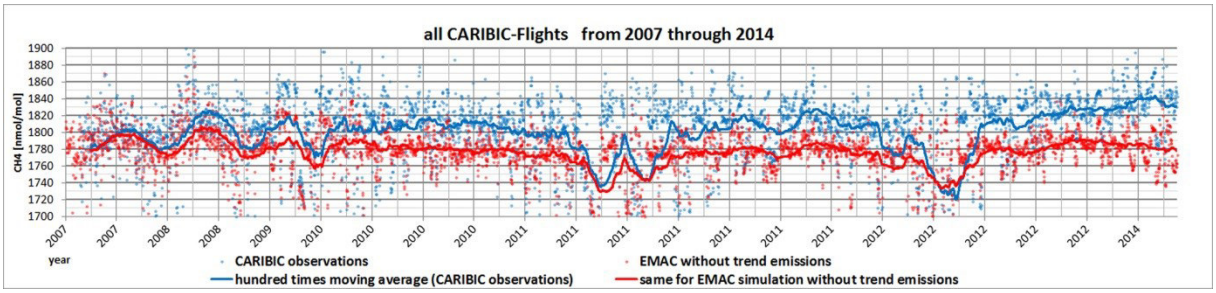

b: same for CARIBIC flights (blue dots) and EMAC simulation without trend emissions (red dots). Superimposed lines represent respective 100 times sliding means for better visibility.

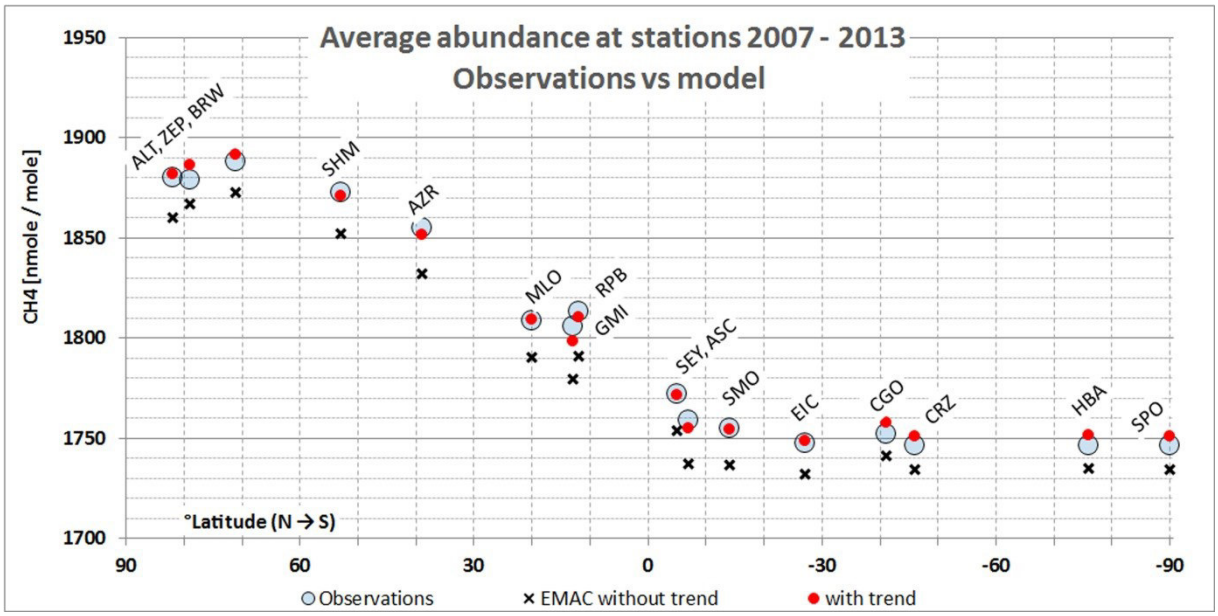

Figure 10: By scaling RIC and TRO emission fractions, the station observations (blue circles) are approximated with smallest RMS: Calculated total CH_4 without- (black crosses), and with optimized trend period emissions (red dots). After 2013, the trend accelerates and additional emission assumptions are necessary.

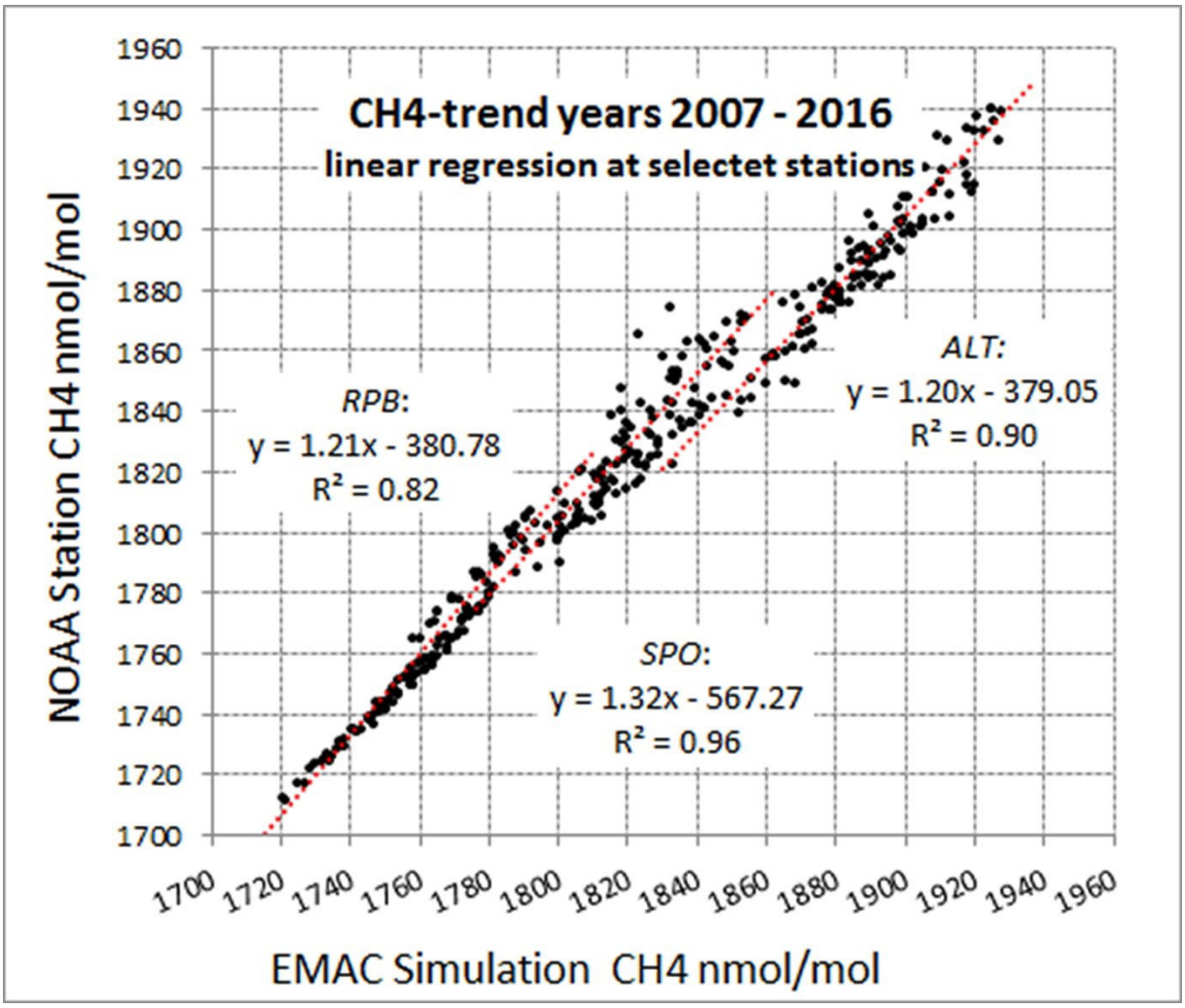

70 Figure 11: Regression analysis of EMAC calculations vs. observations of CH_4 at NOAA stations ALT, RPB, and SPO for the trend years 2007 through 2016.

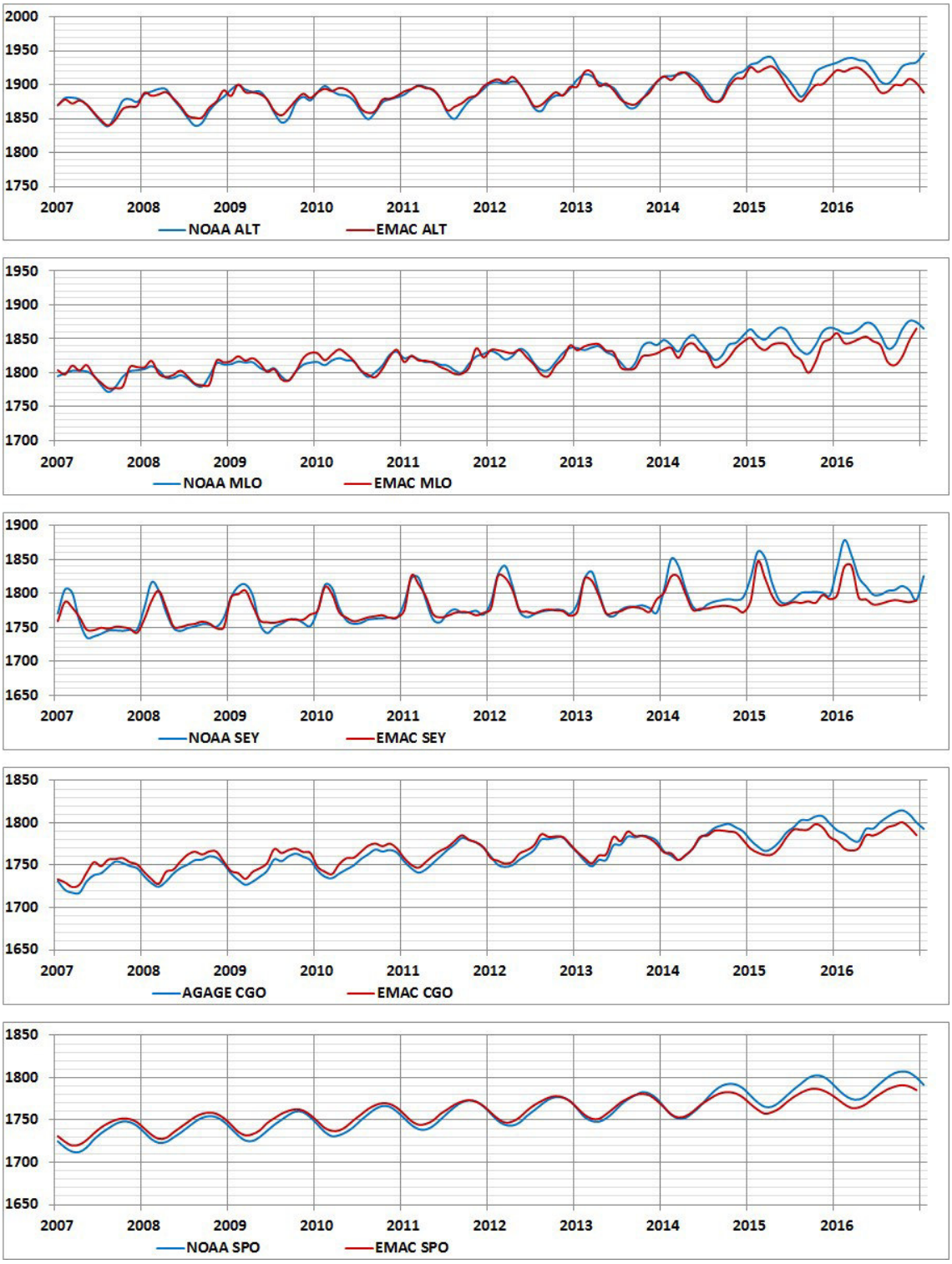

Figure 12: 2007 through 2016 CH_4 development at NOAA and AGAGE stations:
Observations (blue) vs. optimized RIC+TRO (2007 – 2013) emission increment simulations (red).

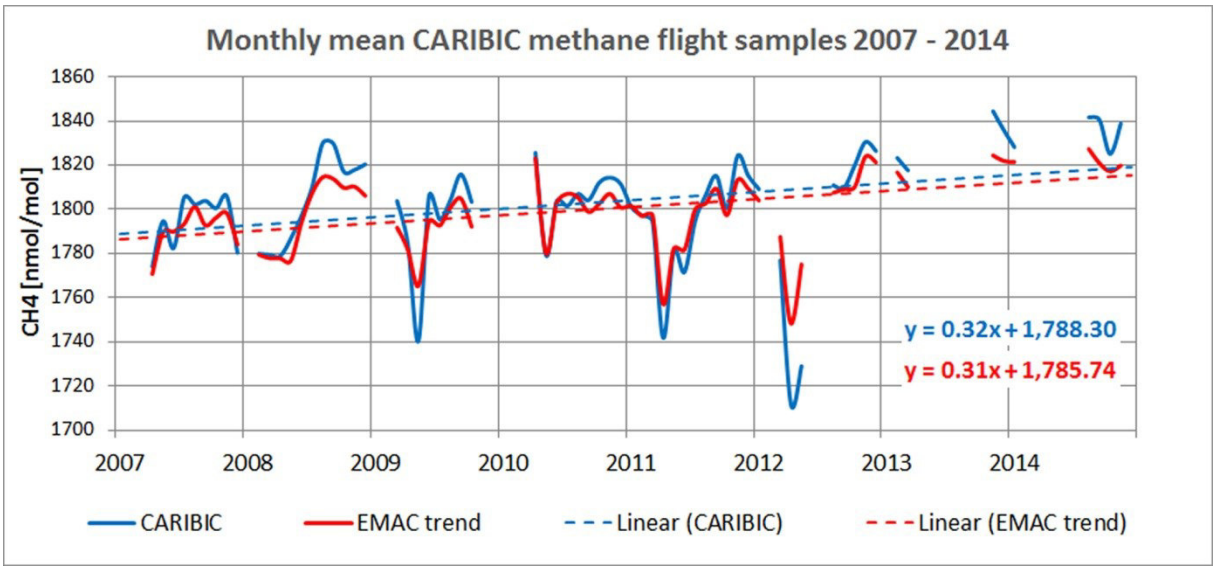

Figure 13: Monthly averaged EMAC-CH_4, including trend and CARIBIC-2 observations 2007 through 2014 for all data obtained from CARIBIC Whole Air Samples (WAS) in blue, and model results in red.

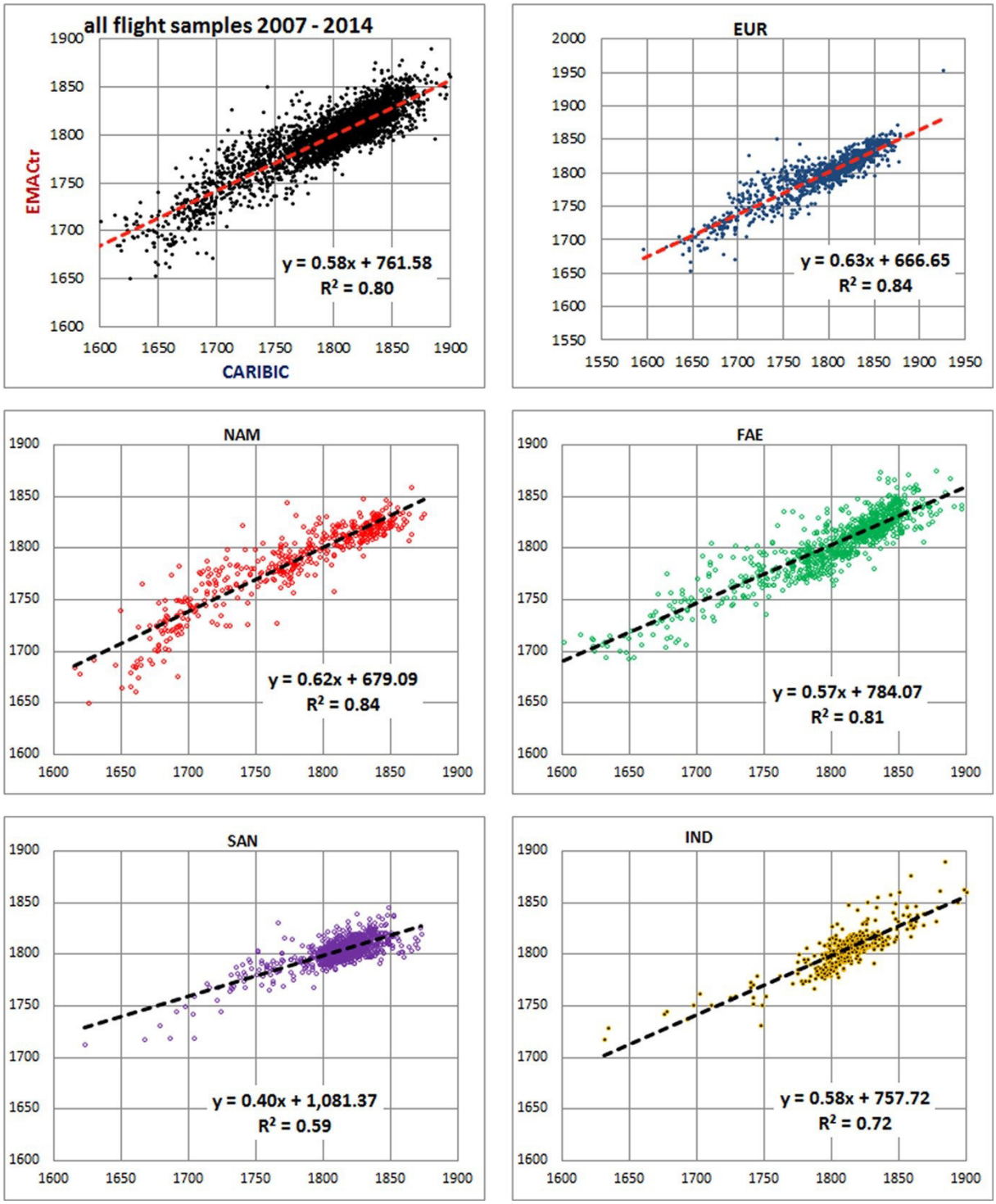

80 Figure 14: Linear regression between CARIBIC-2 samples and EMAC calculations for all trend period flights (2007 – 2014) and for flight regions with more than 300 samples.

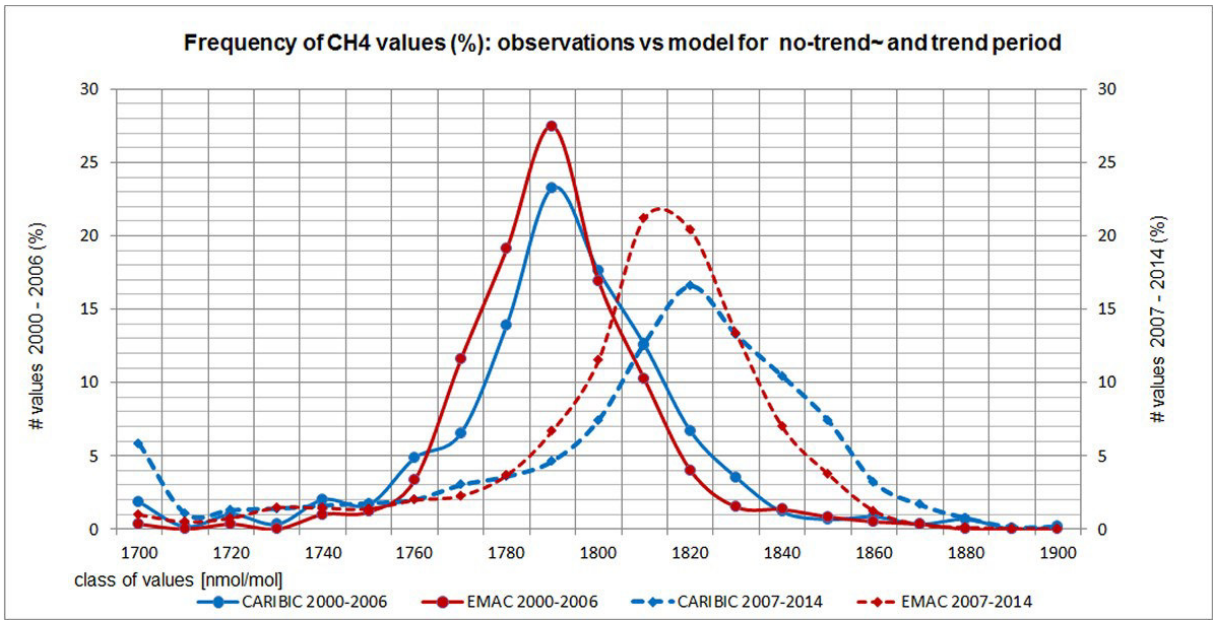

Figure 15: Frequency spectrum of CARIBIC observed and EMAC simulated CH_4-mixing-ratios separately plotted for the years 2000-2006 and 2007-2014.

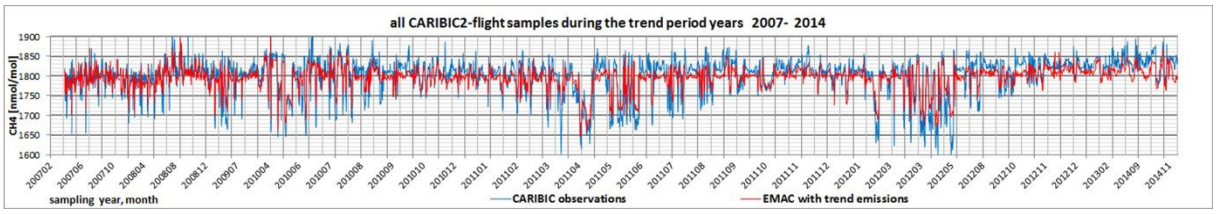

Figure 16:

EMAC CH_4 calculations (red) and CARIBIC-2 observations (blue) from 2007 through 2014 – all flight samples.

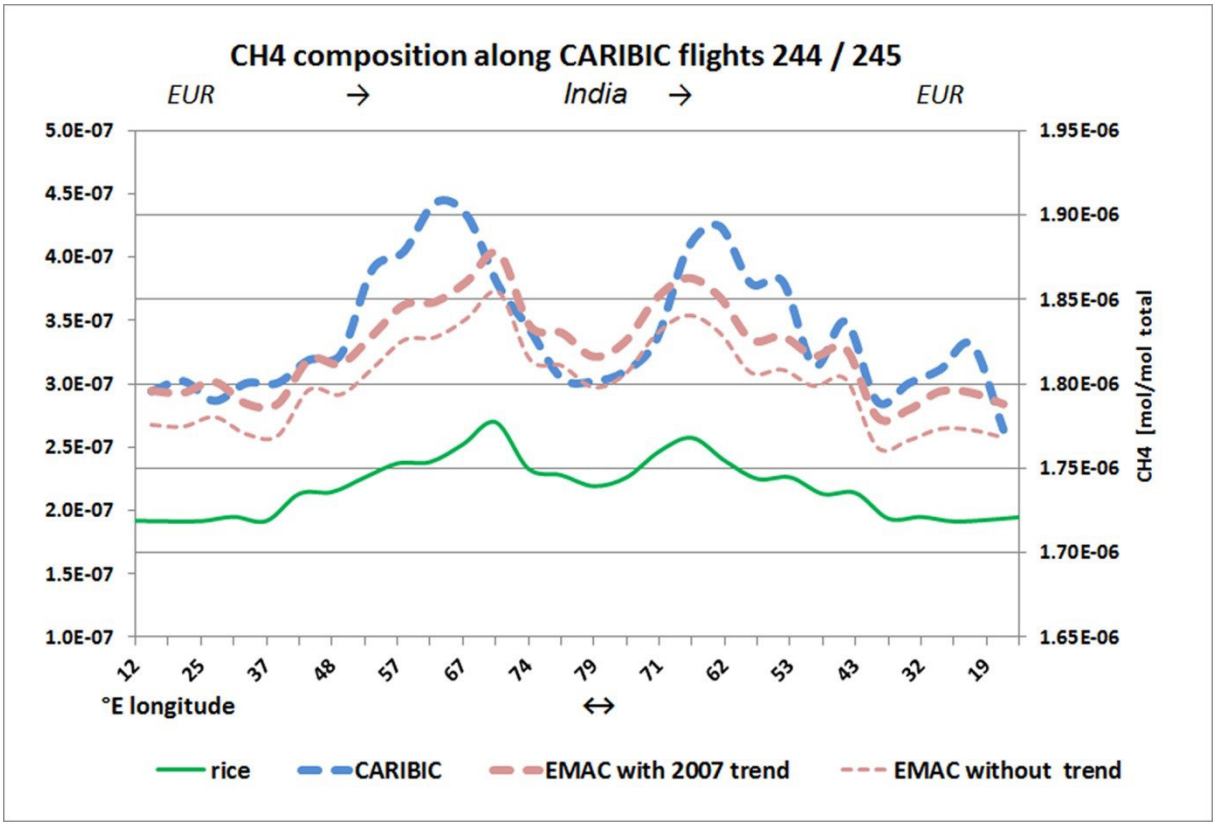

Figure 17:

a: CH_4 mixing ratios observed by CARIBIC (blue dashed, right axis) and calculated by EMAC (red dashed thick) and tagged rice related CH_4 (green, left axis) - India flights Aug. 2008. The thin red dashed line marks the simulation without trend period increment for reference.

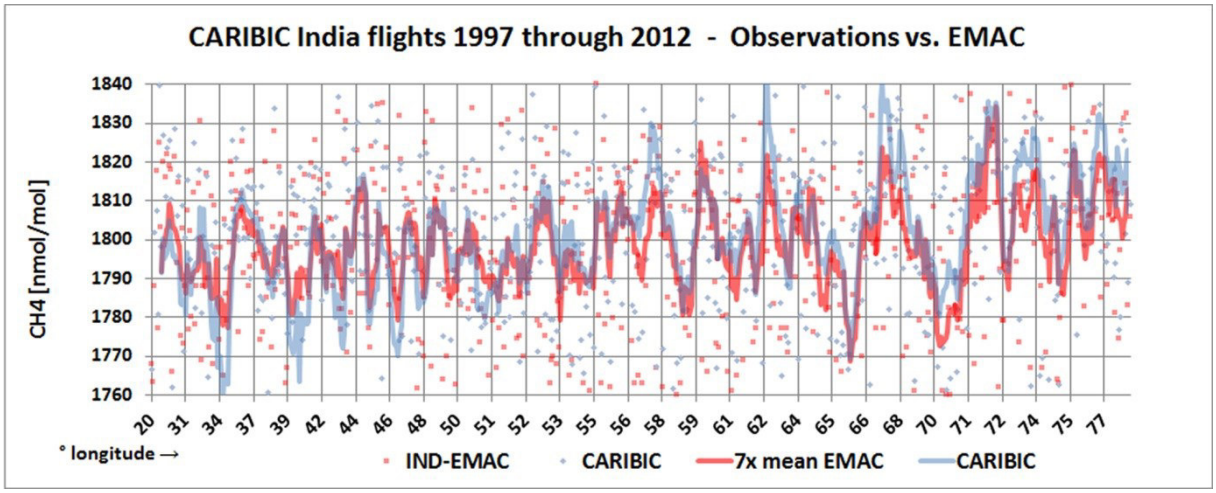

b: CH_4 mixing ratios [nmol/mol] observed by CARIBIC (blue) during all India flights 1997 through 2012 and corresponding EMAC simulations (red). The large scatter requires the sliding average of 7 points (solid lines).